JGR Solid Earth

RESEARCH ARTICLE
10.1029/2022JB025022

Investigating Spectral Estimates of Stress Drop for Small to Moderate Earthquakes With Heterogeneous Slip Distribution: Examples From the 2016–2017 Amatrice Earthquake Sequence

Giovanna Calderoni[1] **and Rachel E. Abercrombie**[2]

[1]Istituto Nazionale di Geofisica e Vulcanologia, Rome, Italy, [2]Boston University, Boston, MA, USA

Key Points:

- Spectral stress drop estimates from different methods do not agree, largely due to ambiguities in separating source and path
- Relative stress drop estimates within each study are more reliable and reflect the high frequency radiation and ground motions
- Finite fault inversions show that corner frequency and stress drop can reflect source complexity rather than actual stress release

Supporting Information:

Supporting Information may be found in the online version of this article.

Correspondence to:

G. Calderoni,
giovanna.calderoni@ingv.it

Citation:

Calderoni, G., & Abercrombie, R. E. (2023). Investigating spectral estimates of stress drop for small to moderate earthquakes with heterogeneous slip distribution: Examples from the 2016–2017 Amatrice earthquake sequence. *Journal of Geophysical Research: Solid Earth*, *128*, e2022JB025022. https://doi.org/10.1029/2022JB025022

Received 29 JUN 2022
Accepted 20 MAY 2023

Author Contributions:

Conceptualization: Giovanna Calderoni, Rachel E. Abercrombie
Data curation: Giovanna Calderoni, Rachel E. Abercrombie
Funding acquisition: Giovanna Calderoni
Methodology: Giovanna Calderoni, Rachel E. Abercrombie
Software: Giovanna Calderoni
Supervision: Giovanna Calderoni, Rachel E. Abercrombie
Validation: Giovanna Calderoni, Rachel E. Abercrombie

Abstract Estimates of spectral stress drop are fundamental to understanding the factors controlling earthquake rupture and high frequency ground motion, but are known to include large, poorly-constrained uncertainties. We use earthquakes from the 2016–2017 sequence in the Italian Appenines (largest event at Norcia, M_w 6.3) to investigate these uncertainties and their causes. The similarly-sized events near Amatrice (M_w 6.0) and Visso (M_w 5.9) enable better constrained relative analysis. We calculate *S* wave source spectra, corner frequencies, and spectral stress drop for 30 of the larger events. We compare both empirical and modeling approaches to isolate the source spectra and calculate source parameters; we also compare our results with those from published studies. Both random and systematic inter-study variations are larger than the standard errors reported by any individual study. The reported magnitude dependence of stress drop varies between studies, being largest for generalized inversions and smallest for more individual event based approaches. The relative spectral estimates of inter-event stress drop are more consistent; all approaches estimated higher stress drop in the Amatrice earthquake than the similar-sized Visso earthquake. In contrast, finite fault inversions of these two earthquakes found that the Visso earthquake had the larger region of concentrated, higher slip, whereas the Amatrice earthquake had multiple, lower slip, subevents. The Amatrice spectra contain more high frequency energy than those of the Visso earthquake. This comparison suggests that consistent measurement of a higher spectral stress drop indicates greater high-frequency ground motion but may correspond to greater rupture complexity rather than higher stress drop.

Plain Language Summary The stress release (or stress drop) during an earthquake is an important element of seismic hazard forecasting; high stress drop earthquakes radiate more high frequency energy, causing stronger ground shaking. The stress drop also provides information about the energy budget, and the size of fault ruptured, and consequently, earthquake triggering and rupture dynamics. Reliable estimates of stress release are difficult to make, largely because of the ambiguity in removing the distorting propagation effects experienced by waves traveling from earthquake to seismometer from recorded seismograms. Most measurements are made using frequency amplitude spectra. We use two methods to estimate earthquake stress drop for 30 of the larger earthquakes in central Italy (2016–2017) and compare them with the results of previous studies. We find that the variation between absolute values estimated in different studies is much larger than the reported formal inversion errors. The relative values are more reliable, with different studies consistently finding a particular earthquake has relatively high or low stress drop. Direct comparison of the similar-sized, damaging Amatrice and Visso earthquakes reveals that the relative spectral stress drop estimates reflect the relative strength of high-frequency ground motion, but may indicate more complex rupture rather than higher average stress release.

1. Introduction

The stress drop in an earthquake is a fundamental factor controlling the rupture dynamics, high-frequency radiation and ground motions (e.g., Kanamori & Brodsky, 2004). Unfortunately, it has become increasingly clear that widely-used spectral stress drop estimates involve uncertainties (random and systematic) that are both large and poorly understood (e.g., Abercrombie, 2021; Baltay et al., 2022). The differences between studies, which depend on the method used and many assumed parameters and data selections, are often much larger than the formal model and inversion errors (e.g., Pennington et al., 2021; Shearer et al., 2019). The main sources of uncertainties are thought to be the separation of source, path and site effects using frequency-limited seismic data, and the assumptions of simplistic source and attenuation models (e.g., Abercrombie, 2021; Ide & Beroza, 2001;

Visualization: Giovanna Calderoni, Rachel E. Abercrombie
Writing – original draft: Giovanna Calderoni, Rachel E. Abercrombie

Pennington et al., 2021; Shearer et al., 2019). Consistent relative variations in spectral stress drop estimates within an earthquake population from independent studies are more robust than the results of any individual study (e.g., Pennington et al., 2021).

Spectral source models all assume a simple, typically circular, rupture, that does not represent the heterogeneous ruptures of real earthquakes, as noted by Madariaga (1979). The slip heterogeneity, also referred to as source complexity, of large earthquakes is well known from finite fault inversions (e.g., Cocco et al., 2016; Mai & Beroza, 2000; Mai & Thingbaijam, 2014; Ye et al., 2016) but a simpler source model was generally thought to be more appropriate for smaller earthquakes. Improved recording is revealing that similar complexity is common in smaller earthquakes (e.g., Abercrombie et al., 2020; Pennington, Chang, et al., 2022; Pennington, Uchide, & Chen, 2022; Uchide & Imanishi, 2016; Yamada et al., 2005), as would be expected from self-similarity. The spectrum of a complex earthquake source will also exhibit a more complex shape than that of a simple circular rupture, with peaks and troughs at frequencies corresponding to the duration and timing of the slip heterogeneity (e.g., Gallovič & Valentová, 2020; Ye et al., 2016). This prompts the question of what simple spectral stress drop estimates are really measuring if an earthquake involves slip heterogeneity. How should these estimates be used to probe earthquake source physics or predict future ground motions? Yoshimitsu et al. (2019) simply excluded any earthquakes with complex spectra from their source parameter analysis which resulted in highly consistent, robust measurements, but the results from such a highly selected subset cannot be considered representative of the earthquake population. Ruhl et al. (2017) and Abercrombie (2014) also tried to separate simple and complex earthquakes in their analysis.

To compare spectral estimates with finite fault models, requires estimating an average stress drop from the heterogeneous slip distributions. Noda et al. (2013) compared various approaches to doing this for a single distribution. Brown et al. (2015) discussed the difficulties of assigning a single "average" stress drop, with uncertainties, for a large, complex earthquake even using a single approach when multiple finite fault inversions are available. How these measurements compare to the results of simple spectral fitting is not well known. Cocco et al. (2016) and others combined results from spectral modeling and finite fault inversion but did not compare the two for individual events; Ye et al. (2016) compared the spectra of their source time functions to standard source spectra, finding significant deviation for more heterogeneous slip distributions, but did not model the spectra. Lin and Lapusta (2018) and Gallovič and Valentová (2020) showed that seismic spectral estimates of stress drop can be poor indications of stress release in an event with a highly complex slip distribution. Abercrombie (2021) demonstrated that the combination of a limited frequency bandwidth and a complex source spectrum can lead to large, systematic variation in stress drop estimates and an artificial dependence of spectral stress drop on seismic moment, if a simple source model is used. This follows from the fact that in spectral source studies covering earthquakes over a range of magnitudes, the signal frequency range above the corner frequency for the large earthquakes is much larger than that below the corner frequency, but the opposite is true for the smaller earthquakes potentially leading to systematic differences in the modeling.

The 2016–2017 damaging central Italy seismic sequence represents an excellent opportunity for investigating earthquake source properties given the high number of earthquakes, the large number of seismic stations, the extended range of magnitude and the extensive area affected by the sequence. The sequence included three mainshocks (Amatrice: *M*6.0, 24 August 2016; Visso: *M*5.9, 16 August 2016 and Norcia: *M*6.3, 30 October 2016) and six other earthquakes with magnitude $M_w > 5$ (Figure 1). Each mainshock ruptured different portions of the NW-SE trending, SW dipping, normal-fault segments that run parallel to the axis of the Apennines Mountain belt (Chiaraluce et al., 2017; Michele et al., 2020). The sequence started with the M_w 6.0 earthquake on 24 August 2016 at 01:36 (UTC) close to the town of Amatrice; the earthquake caused intense ground shaking, the deaths of 299 people and the evacuation of 31,764 more, and also the total destruction of Amatrice's old town. Following two months of continuous aftershock activity, on the 26 October 2016 at 19:18 (UTC) the M_w 5.9 Visso earthquake occurred approximately 30 km NNW of the M_w 6.0 Amatrice earthquake. Four days later, on the 30 October 2016 at 06:40 (UTC), the strongest event of the sequence with M_w 6.3 occurred close to Norcia, roughly halfway between the towns of Amatrice and Visso.

On 18 January 2017, the seismic activity migrated at the south of Amatrice causing further significant damage. In this area eight earthquakes with $M_w \geq 4.0$, four with $M_w \geq 5.0$, occurred within a few hours. The seismicity pattern of the 2016–2017 Amatrice seismic sequence showed the strong interaction between the inherited compressional thrusts and the younger and active normal faults (Barchi et al., 2021).

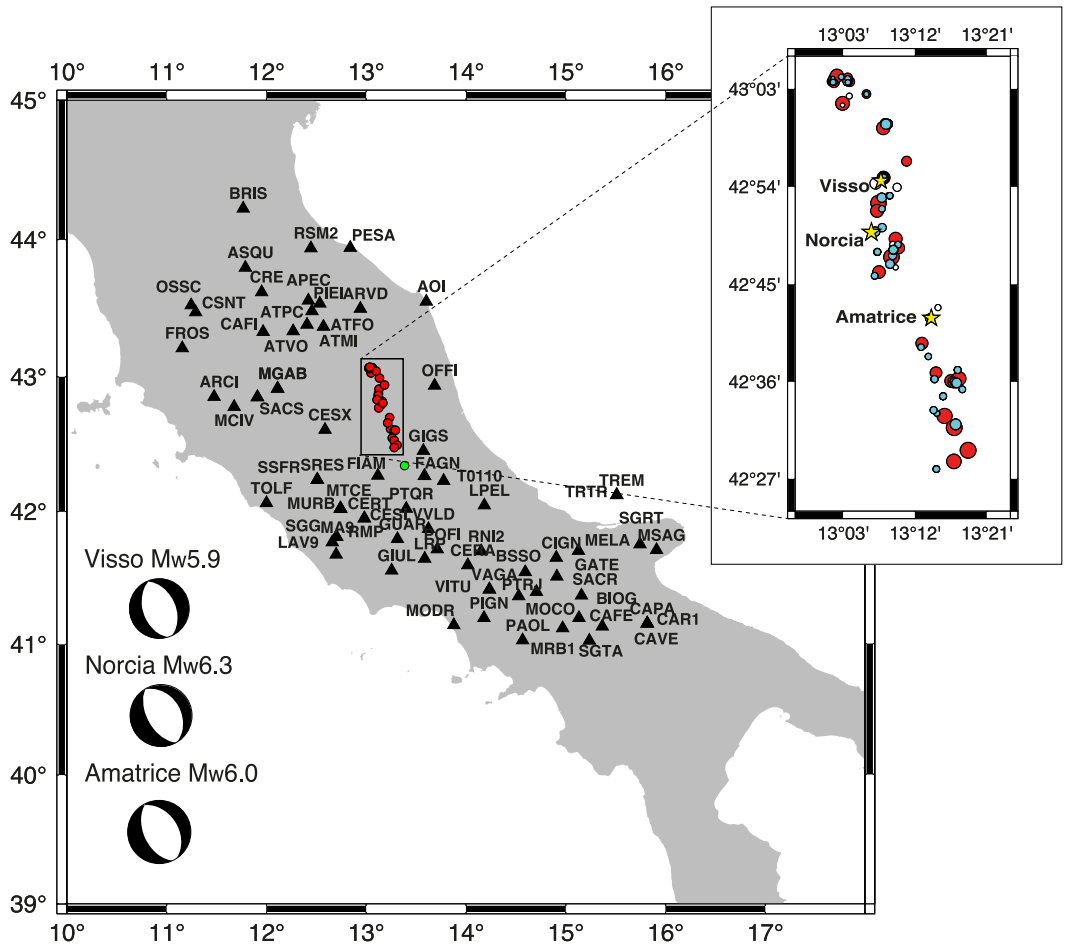

Figure 1. Map showing the location of the earthquakes of this study (red circles), the strongest earthquake that occurred in the same source region during the 2009 L' Aquila seismic sequence (green circle), stations (black triangles) used in the analysis and focal mechanisms from Amatrice, Visso, and Norcia earthquakes are also included. The inset shows the target events with M_w greater than 5.5 (yellow stars), the target events with M_w less than 5.5 (red circles), the empirical Green's function (EGF) included in the selected database (cyan circles), and the EGF eliminated (white circles). All seismic events plotted in the inset are sized by magnitude.

The importance of understanding these earthquakes, and mitigating future hazards led to studies of the stress drop of earthquakes in the 2016–2017 sequence, including those of Morasca et al. (2019), Wang et al. (2019), Bindi, Spallarossa, et al. (2020), and Kemna et al. (2021). There is considerable variability between the results of these previous studies. Morasca et al. (2019), Wang et al. (2019), and Bindi, Spallarossa, et al. (2020) focused on the magnitude scaling dependence, all finding that the larger magnitude earthquakes tended to have higher stress drops, to varying degrees. The exact magnitude range over which this dependence is resolved depends on the limitations of the frequency range of the available data. Previous work has shown that a limited frequency band can lead to scaling artifacts (e.g., Abercrombie, 2021; Chen & Abercrombie, 2020; Ruhl et al., 2017). Kemna et al. (2021) used a different approach and found no magnitude dependence, partly due to different methods, and partly due to different interpretations of the reliable frequency and magnitude ranges. None of these individual analyses investigated specifically why their results differed or agreed with the others.

Kemna et al. (2021) also looked at the spatial and temporal variation of their stress drop estimates; they found them to be related to the segmentation of the fault system with the earthquakes to the south of the Olevano-Antrodoco-Sibillini (OAS) thrust front having relatively low stress drops. The other studies did not investigate either spatial or temporal variability.

Calderoni et al. (2017), Wang et al. (2019), and Colavitti et al. (2022) all investigated the azimuthal directivity of the larger earthquakes in the 2016–2017 Italy sequence and found them to be predominantly unilateral ruptures,

distinctly different from the assumed bilateral circular models of the stress drop studies. Calderoni et al. (2013) and Calderoni et al. (2015) found significant along-strike directivity for earthquakes in the region as small as M3.3, indicating that neglecting directivity in empirical Green's function (EGF) events could also affect results of studies using them to isolate source radiation for larger earthquakes. The kinematic finite-fault inversions of the largest three earthquakes (Chiarluce et al., 2017; Tinti et al., 2016) also revealed significant slip heterogeneity that is likely to affect spectral stress drop estimates obtained assuming simple models. The existence of these models, and also dynamic inversions of the two largest earthquakes (Gallovič et al., 2019; Scognamiglio et al., 2018; Tinti et al., 2021) provide the opportunity to investigate what information absolute and relative spectral stress drops are able to provide about complex ruptures.

Here we use two distinct approaches to measure spectral stress drop from recorded *S* waves and perform a series of tests to investigate the size and relative importance of the uncertainties resulting from the various assumptions made. We then compare our results to those from the previous published studies to quantify variability and look for consistencies. Finally, we compare the spectral measurements of stress drop to the finite-fault models of Tinti et al. (2016) and Chiaraluce et al. (2017) to improve our understanding of what the spectral corner frequency and "stress drop" parameters actually represent when an earthquake is not a simple circular rupture.

2. Spectral Source Parameters

2.1. Theoretical Background

The amplitude spectrum of ground motion at distance R from a seismic source, in this case an earthquake, is the product of the source radiation, the wave propagation, and the contributions from site and instrument:

$$V(f, R) = \Omega_0(\mathrm{f}) \cdot (2\pi f) \cdot A(f, R) \cdot H(f) \cdot I(f) \tag{1}$$

where $V(f, R)$ is the amplitude spectrum of the recorded ground velocity as a function of frequency (f) and distance (R), $\Omega_0(f)$ is the source amplitude spectrum for radiation angles of ϑ and φ, $A(f, R)$ represents the attenuation along the propagation path, $H(f)$ is the site term accounting for attenuation and amplification in the near-surface beneath the station, and $I(f)$ is the instrument response.

Most spectral source modeling is based on assuming a simple circular source model (e.g., Brune, 1970; Madariaga, 1976):

$$\Omega_0(f) = \frac{F_S R_{\vartheta,\varphi}}{4\pi\rho\beta^3} \frac{M_0}{1 + (f/f_0)^2} \tag{2}$$

where M_0 and f_0 are seismic moment and corner frequency, respectively. F_S is the free surface effect, $R_{\theta,\phi}$ accounts for the radiation pattern, ρ is the density, and β the shear-wave velocity.

Estimating earthquake source parameters requires isolating the source term from the other factors. We do this using two different, existing, approaches so we can compare the results; see Abercrombie (2021) for a discussion of some of the advantages and disadvantages of the different approaches.

First, following Anderson and Hough (1984) and Calderoni et al. (2013) we estimate the combined effects of geometrical spreading and crustal attenuation, $A(f, R)$, using

$$A(f, R) = \frac{1}{R} e^{\pi k f} \tag{3}$$

where we assume that geometrical spreading is inversely proportional to distance and that attenuation produces an exponential decay parameterized by a frequency-independent attenuation parameter, κ (Anderson & Hough, 1984; Singh et al., 1982) calculated at each station. We then estimate the site terms $H(f)$ using the approach described by Calderoni et al. (2019). We correct the seismograms at high frequency using Equation 3 and normalize to unit distance. For each event, we average the scaled spectra of available stations and calculate the difference from the mean event spectrum at each station. These differences are averaged over the event ensemble to obtain a mean curve $H(f)$ for each station.

After estimating κ and $H(f)$ we can fit the source spectral shape with Equation 2 to obtain the source parameters.

Second, we use the EGF approach in which a co-located smaller earthquake is assumed to experience the same site and path effects as the event of interest. By dividing Equation 1 for two earthquakes the propagation and instrument terms cancel and we can simply fit the spectral ratio (SR) with the ratio of two source models of type shown in Equation 2.

$$\frac{V_1(f)}{V_2(f)} = \frac{M_{01}}{M_{02}} \cdot \frac{1 + (f/f_{02})^2}{1 + (f/f_{01})^2} \tag{4}$$

For each approach, a source radius (r) and mean stress drop ($\Delta\sigma$) can be calculated from the corner frequency and moment using a circular source assumption (Brune, 1970, 1971; Eshelby, 1957; Keilis-Borok, 1959):

$$r = \frac{0.3724\,\beta}{f_0} \tag{5}$$

$$\Delta\sigma = \frac{7}{16}\frac{M_0}{r^3} \tag{6}$$

The constants in Equations 5 and 6 depend on the assumed source model and rupture velocity (e.g., Kaneko & Shearer, 2014; Madariaga, 1976) and change the absolute values of stress drop (e.g., Abercrombie & Rice, 2005). Using the same values to convert M_0 and f_0 into stress drop allows comparison of relative values between studies, even if the absolute values remain unknown.

2.2. Data

We select for analysis 30 of the largest ($M_w > 3.5$) earthquakes in the 2016–2017 sequence, that are well recorded at multiple stations (Figure 1). This selection includes the 16 $M_w \geq 4.4$ earthquakes previously analyzed for directivity by Calderoni et al. (2017), and also included in most previous spectral stress drop studies. We search for closely located, well-recorded candidate EGF events (following Abercrombie, 2014, 2015) to use in the SR analysis for these target earthquakes, under the additional constraint that for both target and EGF pairs of events the published moment tensors (when calculated) are similar. There are two moment tensor catalogs available for the 2016–2017 sequence, one following Herrmann et al. (2011) and the other following Scognamiglio et al. (2010). We identify 42 potential EGF events ($2.2 \leq M_L \leq 4.05$, between 1 and 5 EGFs for each individual target event) with a magnitude difference range for the pairs between 0.79 and 3.09. For four EGF-target event pairs the source separation is between 7 and 10 km, and for all the others (92%) it is ≤5 km. Table S1 in Supporting Information S2 includes the hypocentral information about the starting data base.

We use the seismograms recorded by the mostly 24-bit broadband 40-s Nanometrics Trillium seismometers of the Italian Seismic Network run by the Istituto Nazionale di Geofisica e Vulcanologia (INGV). We correct all the seismograms using the factory supplied seismometer transfer functions.

From each instrument-corrected velocity seismogram we select a time window for the spectral analysis. For the spectral fitting the time window is calculated to include 95% of the signal (cumulative integral of squared velocity of the horizontal components) duration above noise, after the *S* wave arrival; the time windows range from 10 to 30 s, increasing with event magnitude, and 10% of the window (1–3 s) is before the *S* arrival. For the SR analysis, we select a window of 10 s, starting 1 s before the *S* wave arrivals for all events to facilitate calculation of ratios between earthquakes of different magnitude.

A noise segment having the same duration as the corresponding signal time window is extracted before the *P*-wave arrival. We taper both the noise and signal windows with a 10% cosine filter to calculate the fast Fourier transform. We calculate the geometrical mean of both the noise and signal spectra on the two horizontal components, and then the signal-to-noise ratio (SNR) of the target events and EGFs at each frequency sample. We compute the SNR at all the available stations for each of the selected events, and we only use frequencies at which SNR >3 (Figure S1 in Supporting Information S1).

2.3. Seismic Moment

Seismic moment can be estimated during the spectral fitting (e.g., Bindi, Spallarossa, et al., 2020; Bindi, Zaccarelli, & Kotha, 2020) or independent estimates can be used. Using independent measurements of moment

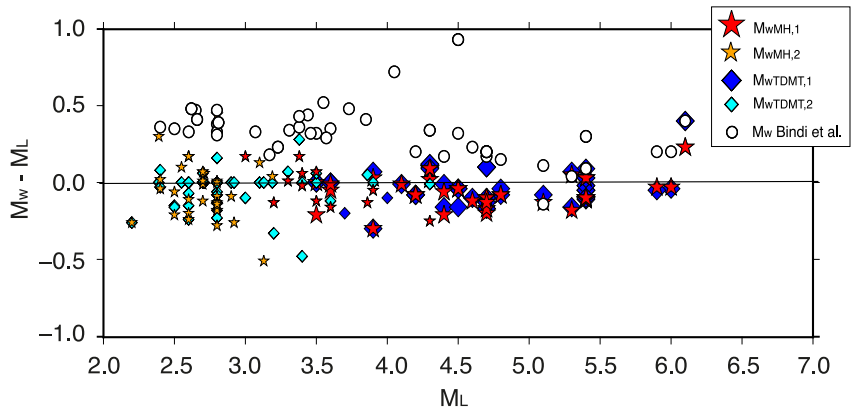

Figure 2. Comparison of moment estimates used and calculated in this study, with those calculated by Bindi, Spallarossa, et al. (2020); Local Magnitude (M_L) is from the Istituto Nazionale di Geofisica e Vulcanologia Bulletin. Large symbols are the 30 target events in this analysis, and smaller symbols show empirical Green's function events in this analysis with moments either in the moment tensor catalogs or calculated here from the low frequency spectral ratios. The two moment tensor catalog estimates are very similar, but the estimates by Bindi, Spallarossa, et al. (2020) are systematically higher, and show a different dependence on M_L.

removes trade-off between corner frequency and moment in both spectral fitting and EGF analyses (e.g., Abercrombie, 2013; Moyer et al., 2018; Walter et al., 2017). As the 30 earthquakes that we analyze are relatively large, we use independently estimated values from regional moment tensor modeling; these methods use the longest period seismic data available and are thought to be most robust. Figure 2 shows that the two available moment tensor catalogs for the sequence have similar dependence on M_L, and no systematic bias. We primarily use the solutions following Herrmann et al. (2011), denoted M_{wMH}, in our analysis. We repeat some of our subsequent analysis for earthquakes also included in the Time Domain Moment Tensor catalog (Scognamiglio et al., 2010), which we denote as M_{wTDMT}, using these solutions to investigate the effects of moment uncertainty. If an EGF earthquake is not included in a particular catalog, we calculate its moment from that of the corresponding target event selected on the basis of the greatest number of stations that recorded the event, and the long period SR, as described below. Figure 2 also compares the moment estimates by Bindi, Spallarossa, et al. (2020); they are systematically higher than the moment tensor values, and show a different dependence on M_L; $M_w - M_L$ decreases with increasing M_L.

2.4. Spectral Fitting

This approach follows that of Calderoni et al. (2019) and involves first calculating the attenuation correction, and then modeling the resulting source spectra.

2.4.1. Calculate Attenuation Correction, κ

To calculate κ for each station we use recordings of the 9 largest earthquakes ($M_w > 5$) in the 2016–2017 sequence, and the strongest earthquake from the 2009 L' Aquila seismic sequence that occurred in the same source region (Figure 1), as they have the best signal to noise over the widest frequency range. Following Calderoni et al. (2019) we model the log-linear spectra of the *S* wave windows on each horizontal component for each event using Equation 2 (Figure 3).

The typical frequency range of the available signals above the background noise is 0.05–25 Hz, but we find that above 10 Hz, the spectra often do not exhibit a constant slope (on a log-linear plot) consistent with a frequency independent κ value. We therefore restrict all our analysis and spectral fitting to a maximum frequency (F_{max}) of 10 Hz. The frequency range of 0.05–10 Hz is relatively large (10 Hz = 0.05 Hz × 200), for example, compared to the 2–25 Hz (25 Hz = 2 Hz × 12.5) available to spectral decomposition studies in California and Oklahoma (e.g., Chen & Abercrombie, 2020; Shearer et al., 2006). We compute the geometric mean κ at each station, and its standard deviation. To check the stability of the κ estimates (Figure 3), we use three different frequency ranges to calculate the κ:

1. FR_0—the widest frequency range: between the low frequency plateau of the displacement spectrum and the limit of SNR (F_{min}; F_{max}) Hz

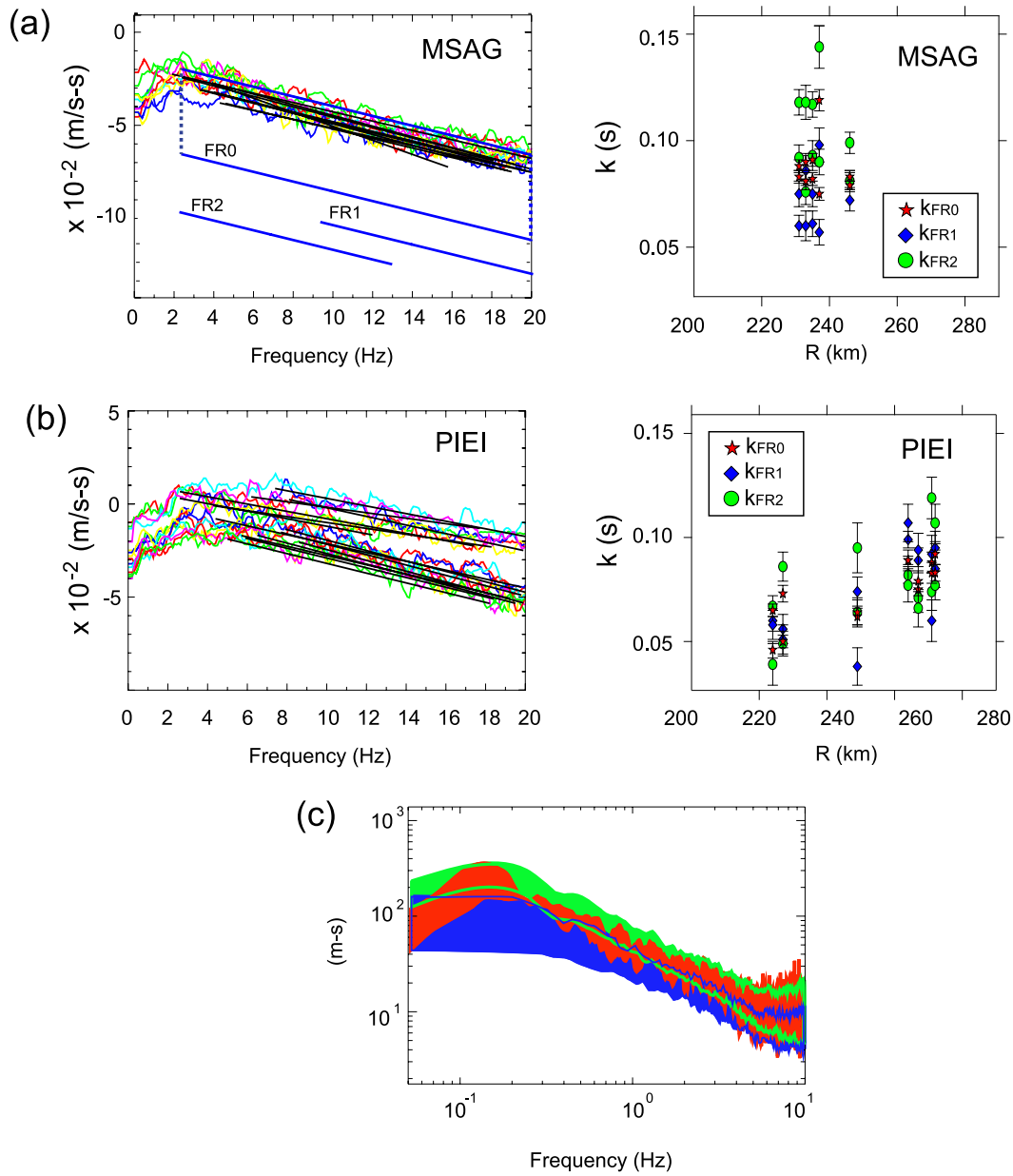

Figure 3. Measurement of attenuation parameter κ in three test frequency ranges: (a, b) show the fits to the spectra for the 10 earthquakes at two different stations (left column), and the resulting estimates of κ for the different frequency ranges (right column). (c) Effects of correcting for κ computed in the different frequency ranges on the velocity spectra ($\pm$1 s.d. band around the average) of the Amatrice earthquake. The velocity spectrum at each station is corrected for geometrical spreading ($1/R$) and station computed κ in the different frequency ranges FR_0 (red), FR_1 (blue), FR_2 (green).

2. FR_1—the higher frequency range: (F_{min} + 1/3 ΔF; F_{max}) Hz with $\Delta F = (F_{max} - F_{min})$
3. FR_2—the lower frequency range: (F_{min}; F_{max} − 1/3 ΔF) Hz

The κ estimates in the three range of frequencies (Figures 3a, 3b and 4a) are similar, although FR_2 yields systematically slightly higher values. We prefer the FR_0 results as they benefit from the stability of the largest frequency range. This approach to estimating κ assumes that the earthquake source acceleration spectrum is constant in the measurement range. The frequency range bands FR_0 and FR_2 may include sufficiently low frequencies to be affected by the finite duration of the sources, but as our preferred results are within 1 standard deviation of those from the higher frequency range (FR_1), we consider this negligible.

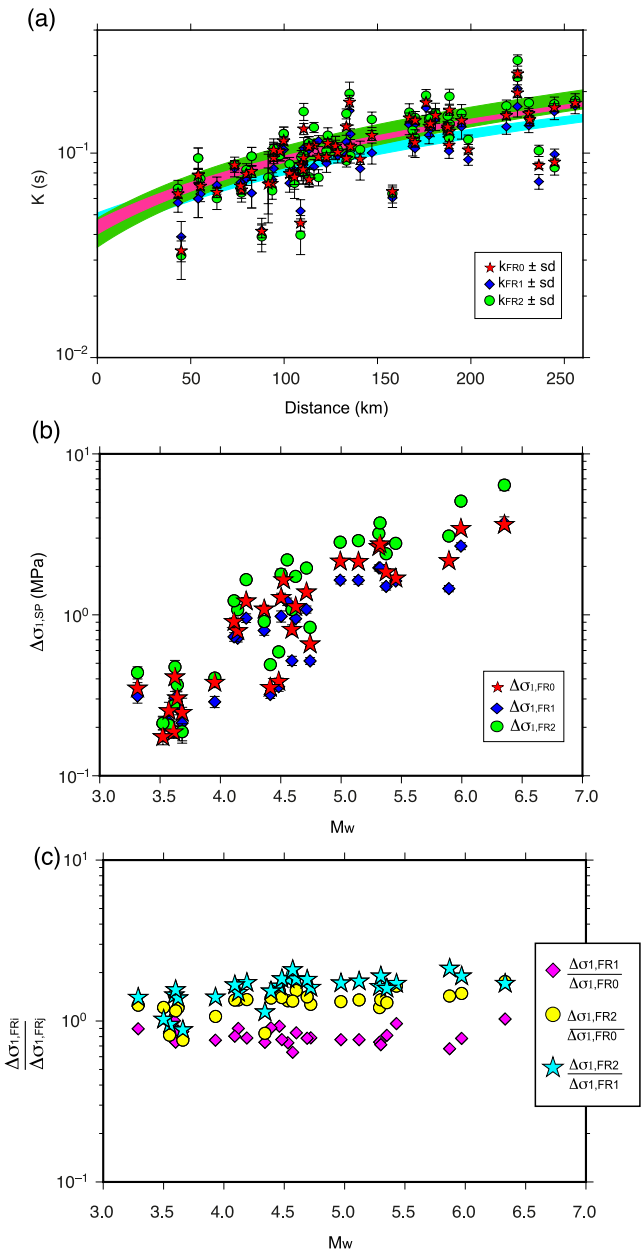

Figure 4. Effects of calculated κ on estimates of stress drop. (a) Three κ values from different frequency ranges (Figure 3) as functions of epicentral distance, error bars are 1 standard deviation; (b) corresponding estimates of stress drop from fitting attenuation-corrected spectra, and (c) ratios of the different stress drops, all calculated using $M_{wMH,1}$. Many error bars are smaller than the symbol size.

2.4.2. Calculate Corner Frequency and Stress Drop

We correct each recorded velocity spectrum using the κ (attenuation parameter) values and the site effect calculated at each station, following the approach developed by Calderoni et al. (2010) and Rovelli and Calderoni (2014). We assume the seismic moments following (Herrmann et al., 2011) and fit the attenuation-corrected spectra with Equation 2, assuming $F_S = 2$, an average $R_{\theta,\phi}$ of 0.55 (Boore & Boatwright, 1984), $\rho = 2800$ kg/m^3 and $\beta = 3{,}100$ m/s from Herrmann et al. (2011). We calculate stress drop using Equations 5 and 6.

Figures 4b and 4c compares the stress drops obtained using the estimates of κ from the three different frequency ranges; $\Delta\sigma_{FR0}$ (using our preferred κ) and $\Delta\sigma_{FR1}$ are the same within a factor of 1.2, but $\Delta\sigma_{FR2}$ is systematically higher, by a factor of 1.8 with respect $\Delta\sigma_{FR0}$. Using the higher frequency κ (FR_1) results in a smaller dependence of stress drop ($\Delta\sigma_{FR2}$) with moment, demonstrating how trade-offs between attenuation and source affect inferences of source scaling. This systematic variation reflects the influence of the radiation and attenuation of high frequency waves on the stress drop estimates; Figure 5 shows the model fits to the spectra using FR_0, for the Amatrice and Visso earthquakes, and a smaller event as examples. Using a different moment estimate for these calculations would not affect the shape of the amplitude spectra, or the relative stress drop estimates, but simply cause a linear change in absolute stress drop estimated, similar to assuming an alternative source model (e.g., Abercrombie & Rice, 2005) and constants in Equations 5 and 6.

2.5. Spectral Ratios

To investigate any dependence of calculated stress drop on analysis method, we recalculate the stress drops for the same 30 earthquakes, using the same raw S wave spectra, using an EGF approach. Before computing the SR, we interpolate the numerator and denominator spectra using logarithmic sampling to decrease the weighting toward the higher-frequency part of the spectra (e.g., Abercrombie, 2021; Ide et al., 2003) and smoothed with a 0.2 Hz wide triangular operator. Calculating the SR between target and EGF events eliminates the propagation and site terms (Equations 1 and 4) and provides the ratio of the source terms.

Rather than inverting the spectral ratios for the moment ratio, we use independent measurements of seismic moment (made at longer periods for the larger event) to decrease the number of unknowns, and improve the stability of the results (e.g., Walter et al., 2017). The ratio of the moment values affects the corner frequency measurements and so we repeat the SR fitting using both moment tensor catalogs (Figure 2) to investigate the uncertainties.

Some EGF events are too small to be included in either one or both moment tensor catalogs. We could attempt to fit the three unknowns (M_{02}, f_{01}, f_{02}) together in these instances but we prefer to first estimate the moment ratio, using different frequency ranges, and making various specified assumptions about the corner frequencies, to understand better the trade-offs between the parameters.

If the EGF event is not included in the moment-tensor catalog, we estimate M_{02} from the ratio of the low-frequency displacement plateau to the known M_{01} of the target event. We use the frequency range $F_{min,EGF}$ to $F_{cTargHP}$, where $F_{min,EGF}$ is the minimum frequency with SNR >3, and $F_{cTargHP}$ is an estimate, by visual inspection, of where the amplitude of the SR starts to decrease. We estimate the best fit values of M_{02} through a grid search procedure (Equation 6) where M_{01} is known and f_{01} and f_{02} are written in terms of seismic moment and stress drop

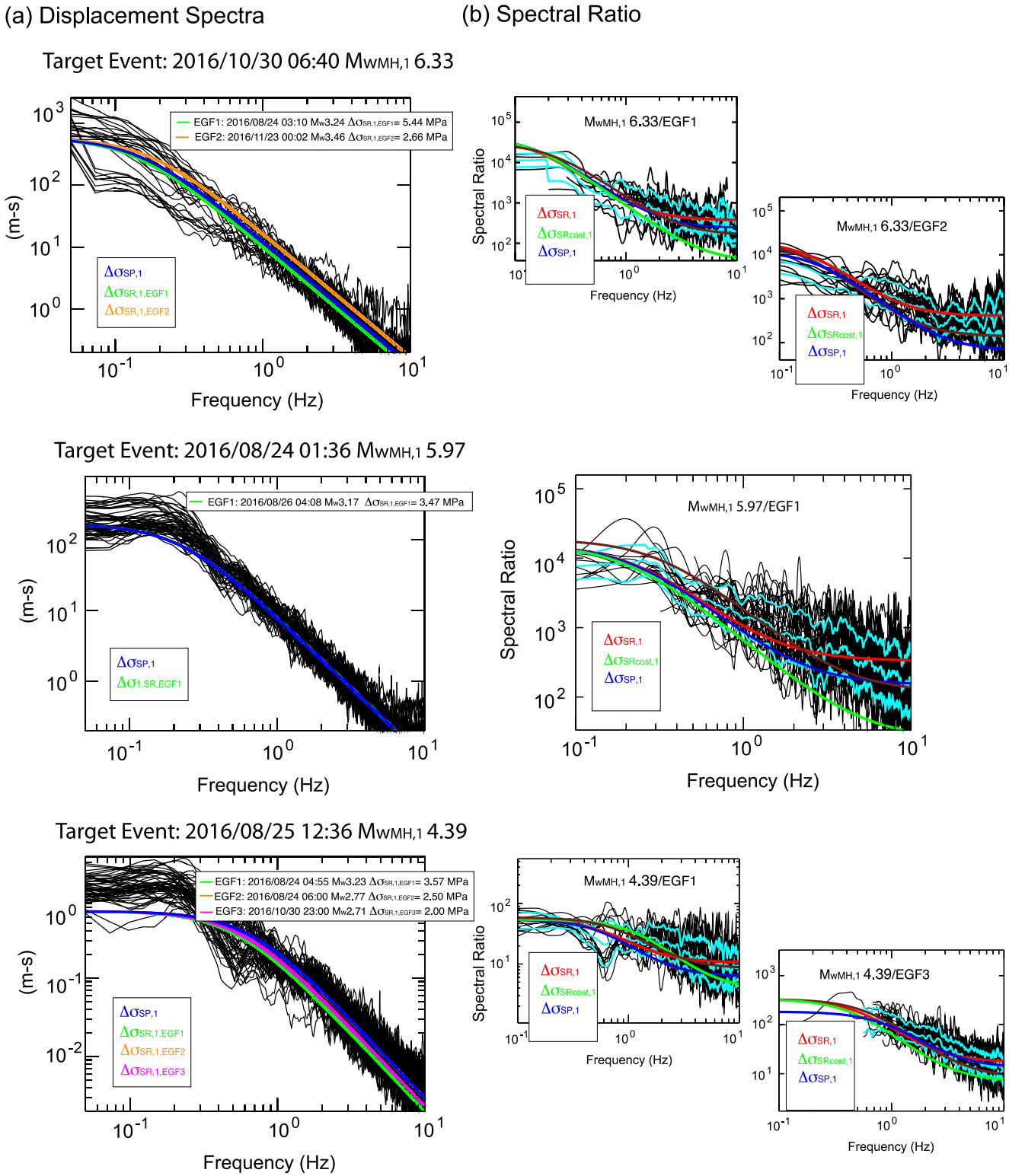

Figure 5. Comparison of different calculated source spectra and spectral ratios with the observed data. (a) Displacement spectra corrected with appropriate κ at each station (FR_0) and geometrical spreading of $1/R$ (Equation 3), overlain with the different theoretical models from the spectral fitting ($\Delta\sigma_{SP,1}$), and from every spectral ratio (SR) (Target/EGF1: $\Delta\sigma_{SR,2,EGF1}$, Target/EGF2: $\Delta\sigma_{SR,2,EGF2}$, …). (b) Spectral ratios with the different theoretical model from fitting spectra ($\Delta\sigma_{SP,1}$), SR ($\Delta\sigma_{SR,1}$), SR with constant stress drop ($\Delta\sigma_{SRcost,1}$), and Bindi, Spallarossa, et al. (2020), Bindi, Zaccarelli, and Kotha (2020) ($\Delta\sigma_{B,1}$). In the top left side, the Norcia earthquake M_w 6.33; in the top right side SR of Norcia and EGF with M_w Bindi known. In the middle left side, the Amatrice M_w 6.0; in the middle right side the same of upper; In the bottom right side the small earthquake M_w 4.36.

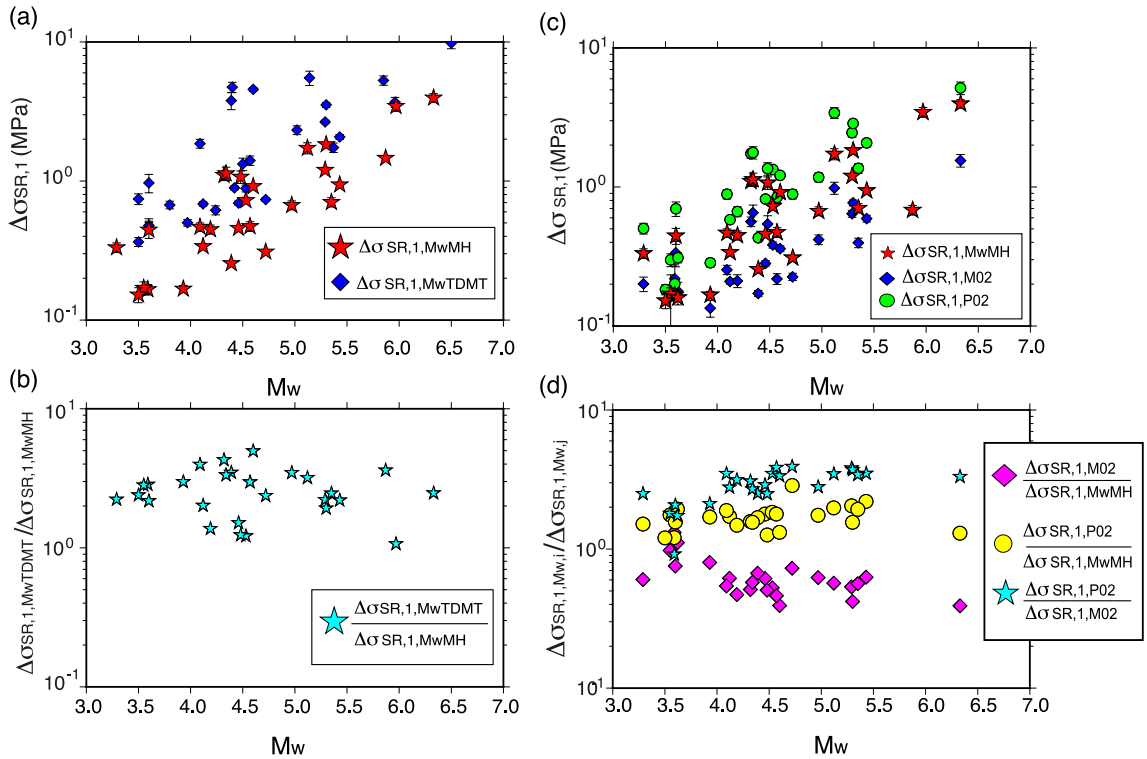

Figure 6. Effects of moment estimates on the stress drop measurements made from the spectral ratios. (a) Stress drops from modeling our preferred frequency ranges and the two different moment catalogs, and (b) the ratios of these stress drops. Varying the frequency range used to estimate the moment of the EGF event corresponds to changes in M_{w2} of 0.2. Therefore, we add and subtract 0.2 from M_{w2} and recalculate the stress drops to determine the effects on the resulting stress drops from the spectral ratios. (c) Calculated stress drops: $\Delta\sigma_{SR,1,MwMH}$ (red stars) use M calculated in our preferred frequency range, $\Delta\sigma_{SR,1,P02}$ (green circles) add 0.2 magnitude units the M_{w2} ($M_{w2,P2} = M_{w2} + 0.2$) $\Delta\sigma_{SR,1,M02}$ (blue diamonds) subtract 0.2 magnitude units M_{w2} ($M_{w2,M2} = M_{w2} - 0.2$), and (d) ratios of these stress drops.

(Equations 4 and 5). As a starting approximation we estimate $\Delta\sigma_{SR,2}$ and $\Delta\sigma_{SR,1}$ using the scaling law deduced by Calderoni et al. (2013). To eliminate the problem due to the bandwidth limitations, we choose a seismic event located within approximately one source dimension of the EGF with magnitude in the range from 4 to 5, except for the M_{02} of the Visso earthquake EGFs.

We then use these moment values to estimate $\Delta\sigma_{SR,1}$ in the frequency range in which both spectra are above the signal to noise threshold, $F_{minNEGF}$ to $F_{maxNEGF}$, by performing a double loop inversion (Equation 4). In the first step, the best fit values of $\Delta\sigma_{SR,1}$ and $\Delta\sigma_{SR,2}$ are estimated through a grid search procedure where M_{01} and M_{02} are fixed; in the second step, the best fit value of $\Delta\sigma_{SR,1}$ is estimated through a grid search procedure where M_{01}, M_{02} and $\Delta\sigma_{SR,2}$ are fixed. $\Delta\sigma_{SR,1}$ is computed as the weighted average over target-EGF pairs. This approach is similar to applying a constraint to f_{02} (e.g., Pennington et al., 2021) to avoid the trade-offs observed by Shearer et al. (2019).

We use five different tests to investigate the effects of the different data and parameter choices in the analysis.

1. We repeat the analysis using both moment tensor catalogs to investigate how the choice of the moment magnitude ($M_{wTDMT,1}$ $M_{wMH,1}$) affects the $\Delta\sigma_{SR,1}$; examples of the results for specific events are shown in Figure S2 in Supporting Information S1. Figure 2 compares the different moment estimates, and Figures 6a and 6b shows their impacts on stress drop estimates.
2. We find that varying the choice of frequency range used to calculate the moment of the EGF event corresponds to changes in M_{w2} within 0.2 units (see examples in Figure S2 in Supporting Information S1). We investigate the effects of such variation in the moment ratio on the resulting stress drop by adding and subtracting 0.2 M units to M_{w2} and repeating the analysis (Figures 6c and 6d). Increasing M_{w2} by 0.2 units can decrease the stress drop of the target stress drop by up to a factor of 2 (Figure 6b).
3. The choice of the EGF used in the SR also affects the resulting $\Delta\sigma_{SR,1}$ estimates (e.g., Abercrombie, 2015). We consider the potential EGFs and select the best based on the frequency range with good SNR, and how well

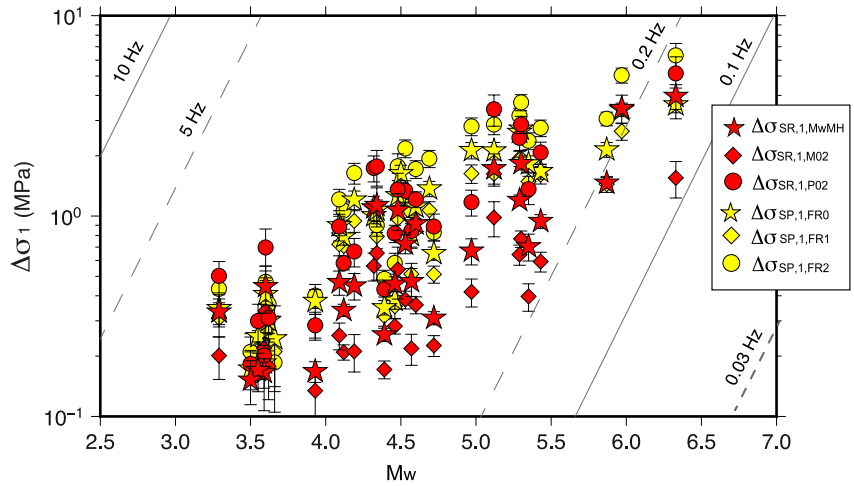

Figure 7. Comparison of stress drop estimates from both spectral fitting and spectral ratio approaches, with different assumptions, to show the variability not included in the formal model fitting errors. The error bars are two standard deviations. Many error bars are smaller than the symbol size. Gray lines indicate the data bandwidth limitations: solid lines are assuming the minimum (0.1 Hz) and maximum (10 Hz) frequencies are the corner frequencies, dash lines assume resolvable corner frequency range is within a factor of two of the limits (0.2 and 5 Hz).

the spectral ratios and displacement spectra fit the circular source model. Examples of the effects of different EGF are shown in Figures S3 and S4 in Supporting Information S1.

4. EGF directivity effect (Figures S4 and S5 in Supporting Information S1). When the difference between the $\Delta\sigma_{SR,1}$ and $\Delta\sigma_{SP,1}$ is greater than a factor of 2.5 for an individual EGF it is likely that the EGF itself involves significant directivity, and so these EGF events are excluded (e.g., see Figure S4 in Supporting Information S1).
5. Choice of frequency range SNR $\geq$ 0.2 Hz and SNR $\geq$ 0.05 Hz on the $\Delta\sigma_{SR,1}$ and $\Delta\sigma_{SP,1}$ (Figures S6 and S7 in Supporting Information S1). The frequency range has a greater influence on $\Delta\sigma_{SR,1}$ estimates especially for the larger magnitude events ($M > 4$) which need lower frequency signal to resolve the corner frequency.

These tests show that the uncertainties resulting from the input assumptions, and choices of data and analysis are larger than the formal model errors; the error bars from the different tests do not overlap in Figures 4b, 6a–6c, and 7. From our starting database of 30 large events and 49 EGFs (all target-EGF pairs in Table S1 in Supporting Information S2), we obtain results for 29 target events and 41 EGFs using the SR approach (target-EGF pairs in bold text in Table S1 in Supporting Information S2).

We also check the influence of the focal mechanisms of the target-EGF pairs on the stress drop estimates (Table S2 in Supporting Information S2); all the earthquakes involve predominantly normal faulting. As shown in the Table S2 in Supporting Information S2 the stress drop estimates are quite similar even when there is some difference between focal mechanisms of the target-EGF pairs. Differing focal mechanisms will have most effect for stations close to nodal planes and so we suspect the large number of stations and good azimuth coverage (Figure 1) reduces the effect of the focal mechanism of EGFs on stress drop estimates in this study.

3. Results of Spectral Source Analysis, and Comparison With Previous Studies

We compare the stress drop measurements we make using the spectral fitting and SR approaches in Figure 7. There is a lot of variability and, as shown in the preceding sections, data selection choices and assumptions used in the different methods have a significant effect both on absolute values, and the relative values and magnitude dependence. There is a spread of approximately a factor of 4 in stress drop for each event that does not include any dependence on source model constants, or rupture velocity which are assumed the same throughout. All the approaches reveal some increase in spectral stress drop with moment; the SR method results in a lower scaling dependence than the spectral fitting, although using only the higher frequency estimate of attenuation would decrease the scaling dependence from the latter (Section 2.4).

An artificial apparent increase in estimates of spectral stress drop with moment is known to result from imperfect correction for attenuation (e.g., Ide et al., 2003) and also from the use of the limited frequency of the available

data (e.g., Ruhl et al., 2017). We indicate the stress drops corresponding to the minimum and maximum frequencies used in the SR fitting (solid gray lines), and also use dashed gray lines to indicate the likely resolvable limits for corner frequency based on the work of Ruhl et al. (2017) and Chen and Abercrombie (2020). Our spectral measurements are well-resolved by these recommended criteria, but the possibility of systematic bias in a data set, remains, as a direct consequence of the modeling of the larger earthquakes being dominated by frequencies above the corner frequency and that of the smaller events being dominated by frequencies below the corner frequency (Abercrombie, 2021).

3.1. Comparison With Previous Studies: Stress Drop Scaling With Moment

In Figure 8 we compare our preferred results using each of the two methods (Table S3 in Supporting Information S2), to those of the previous published studies; Figure 5 and Figures S8 and S9 in Supporting Information S1 show examples of how the different models match the observed data. To ensure meaningful comparisons in Figure 8 we recompute the spectral stress drops from the published moment and corner frequency values, using the same constants in Equations 5 and 6 as we use in our own analysis (Table S4 in Supporting Information S2). Figure S10 in Supporting Information S1 includes the effects of using different moment estimates. The systematic and random uncertainties in both moment and corner frequency are far larger than the formal reported uncertainties (which do not overlap for individual events between studies) from the individual inversion methods. The different approaches result in different average stress drop values, varying over a factor of 10, and also different dependence on magnitude.

Morasca et al. (2019) analyzed 83 earthquakes using the coda wave ratio approach of Mayeda et al. (2007). They fixed the moments to those of Herrmann et al. (2011) as we do but obtained higher corner frequencies and stress drops (Figure 8 and Figure S10 in Supporting Information S1). Bindi, Spallarossa, et al. (2020) performed a large-scale generalized inversion of over 4,111 earthquakes (M 1.5–6.5) in which they inverted for attenuation together with moment and corner frequency. This approach yields the strongest increase in stress drop with magnitude of those shown in Figure 8. The seismic moments estimated by Bindi, Spallarossa, et al. (2020) are systematically larger than those from the moment tensor catalogs (Figure 2) and also exhibit a different relationship to the INGV catalog magnitude. The generalized inversions tend to be relatively stable as they include large numbers of earthquakes but are subject to trade-offs between moment and corner frequency, and also between spatial variation in attenuation and source effects within the inversion volume (e.g., Abercrombie et al., 2021; Bindi et al., 2021). In a follow-up study, Morasca et al. (2022) combined the generalized inversion technique with the coda wave approach of Mayeda et al. (2003) to investigate the trade-off between moment and corner-frequency. They obtained moment estimates comparable with those of Herrmann et al. (2011), and stress drops more comparable to the ones determined here for the largest events.

Kemna et al. (2021) used three increasingly well-constrained approaches to obtain independent estimates of stress drop for earthquakes from the sequence: individually fitting the spectra for source and attenuation (16,000 earthquakes M_L 0.6–6.5), then a clustering approach with spatial constraints on attenuation, and a SR method for smaller subsets of events. In contrast to the other studies, they obtained stress drops that are independent of the seismic moment, above $M_L 3$, and interpret the apparent decrease in stress drop at smaller magnitudes as a consequence of measurement bias using band-limited data.

In addition to comparing the estimated stress drop values directly, we also investigate how well the different source models fit the recorded data. We calculate the model spectra using the parameters calculated in the different studies and compare them to the attenuation-corrected spectra and the spectral ratios; Figure 5, Figure S8, and S9 in Supporting Information S1 show some examples. The variability of the observed spectra and ratios is large compared to the difference between the different model predictions suggesting the real uncertainties are much larger than predicted. All the SR models (assuming simple circular rupture) with non-constant stress drop fall within 1 standard deviation of the inter-station variation for these earthquakes.

The same moments for the target and EGF earthquakes are used for both the SR ($\Delta\sigma_{SR,1}$) and spectral fitting ($\Delta\sigma_{SP,1}$) methods applied in this study. The seismic moment estimates from Bindi, Spallarossa, et al. (2020) are systematically different (Figure 2 and Figure S11 in Supporting Information S1) leading to systematically lower amplitudes for the predicted low-frequency spectral ratios (see the blue curves at low frequency in Figure 5b). This could result from trade-offs between the attenuation correction, and the seismic moment and corner frequency, and hence resolution of scaling.

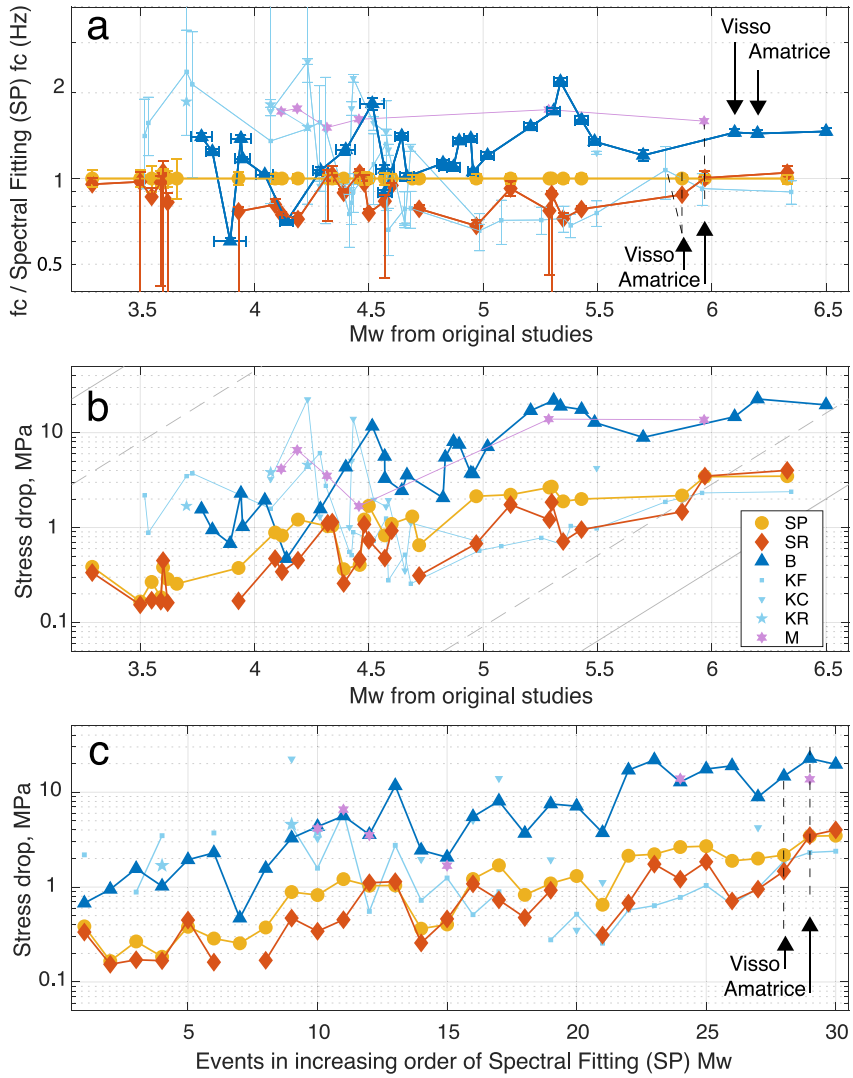

Figure 8. Comparison of preferred spectral ratio (SR) and spectral fitting (SP) estimates from this study, with previously published results; (b) Bindi, Spallarossa, et al. (2020), M: Morasca et al. (2019), and KF, KC, and KR: spectral fitting, cluster analysis and spectral ratios respectively, from Kemna et al. (2021). (a) Comparison of calculated corner frequencies to those of the SP in this study, plotted against the M_w used in the individual study. (b) Stress drop calculated from published f_c and M_0 using the same constants as in our analysis (Equations 5 and 6). Gray lines indicate the data bandwidth limitations: solid lines are assuming the minimum (0.1 Hz) and maximum (10 Hz) frequencies are the corner frequencies, dash lines assume resolvable corner frequency range is within a factor of two of the limits (0.2 and 5 Hz) (c) Calculated stress drop, as in (b), but plotted by event to ease comparison. Compare to Figure S9 in Supporting Information S1 to see effects of assuming same moment for <each event and removing moment trend. The error bars are twice the standard deviation calculated in the modeling.

In common with most previous studies of this earthquake sequence, we find that the earthquakes $M > 5$ tend to have higher spectral stress drops than the smaller events. In Figure 8, most studies, including ours and that of Bindi, Spallarossa, et al. (2020) also exhibit an increase in spectral stress drop with moment in the $M3$–5 range. In their larger data set, however, Bindi, Spallarossa, et al. (2020) observed little dependence of spectral stress drop on magnitude in the range M_w3–5, suggesting that the increase seen in Figure 8 in this magnitude range may be an artifact of the selection of the relatively small number of events we study here.

To investigate resolution of stress drop scale dependence, we also fit the spectral ratios assuming identical stress drop for target and EGF earthquakes (Figure 5, Figures S8 and S9 in Supporting Information S1); these models have consistently poorer fits (and also one less degree of freedom), with the model high frequency level systematically toward the lower range of the data, but they are within the range of the data for many event pairs. The

results from both methods used here show an increase in spectral stress drop with moment that varies with analysis choices; the relationship is not obviously an artifact of observational limitations, but the trade-offs are large and assumptions significant (e.g., Abercrombie, 2021) so we interpret the trends in Figure 8 and Figure S10 in Supporting Information S1 with caution.

Increase in spectral stress drop with moment has been reported within specific magnitude ranges, in individual studies, but trends like the ones observed here cannot extend over a large magnitude range without producing values for smaller and larger earthquakes far outside the observations (e.g., Abercrombie, 1995; Ide & Beroza, 2001; Salvadurai, 2019). The relation between the spectral measurements and the actual stress release during an earthquake is also not straightforward if the source deviates from a simple, circular rupture, for example, a different aspect ratio producing multiple corner frequencies (Ji & Archuleta, 2020, 2022), or other slip heterogeneity (Abercrombie, 2021). The availability of finite-fault models for the largest earthquakes in our analysis enables us to investigate this further in the Section 4.

3.2. Spatial Variation in Stress Drop

Despite all this variability, there are also some strong consistencies observable in Figure 8 with individual events having relatively high (or low) stress drop estimates in all studies. For example, in Figure 8c all studies show event 13 to have a higher stress drop than event 15. Following Pennington et al. (2021) we consider relative values that are consistent using multiple methods and studies to be the most reliable parameters.

Kemna et al. (2021) reported distinct spatial variation in stress drop during the 2016–2017 sequence, but Bindi, Spallarossa, et al. (2020) did not investigate the spatial variation of stress drop and the other studies analyzed relatively few events. We plot the spatial variation of our calculated spectral stress drop values in Figure 9 and observe that they are consistent with the pattern reported by Kemna et al. (2021). Earthquakes to the north of Visso, and also just to the south of the OAS thrust front, have lower stress drops. The seismicity pattern of the 2016–2017 Amatrice seismic sequence also shows strong interaction between the inherited compressional thrusts and the younger and active normal faults. To investigate whether the fault geometry and segmentation have direct effects on the earthquake sources would require more detailed analysis of a larger number of earthquakes, with careful consideration of the trade-off between depth-dependent attenuation and source (Abercrombie et al., 2021).

4. Comparison With Finite Fault Inversions

The three largest earthquakes have all been modeled extensively using finite fault analyses, providing the opportunity to investigate how spectral stress drop estimates compare to independent estimates of rupture area, slip heterogeneity and stress release. We can compare the spectral stress drop estimates directly with the average stress drop in the dynamic rupture models of the two largest earthquakes. Gallovič et al. (2019) obtained an average stress drop of about 4 MPa for the Amatrice earthquake, and Tinti et al. (2021) determined an average stress drop of 2–4 MPa for the Norcia earthquake. These values are comparable to the spectral stress drops obtained here, and by Kemna et al. (2021) and Morasca et al. (2022), but significantly smaller than those of Bindi, Spallarossa, et al. (2020) and Morasca et al. (2019). As we assume the Brune (1970, 1971) source model, which has the highest value for k in Equation 5 of standard spectral models (e.g., Kaneko & Shearer, 2015; Madariaga, 1976) simply using a different spectral source model would increase all the spectral stress drop values.

The Amatrice and Visso earthquakes are very similar in magnitude, and so present a good opportunity to compare relative spectral estimates of source dimension and stress drop, with existing finite fault models without needing to consider magnitude dependence or different levels of resolution. All the spectral studies report a lower stress drop, by a factor of between 1.5 and 2, for the Visso mainshock than the Amatrice mainshock (events 28 and 29 respectively in Figure 8c). The difference is small compared to the known uncertainties, but it is consistent across multiple methods and studies.

Tinti et al. (2016) and Chiaraluce et al. (2017) inverted strong motion seismograms recorded at distances less than 45 km for kinematic rupture models of the Amatrice and Visso earthquakes, respectively. They followed the approach of Hartzell and Heaton (1983), Dreger and Kaverina (2000), and Dreger et al. (2005), and band-pass filtered the data between 0.02 and 0.5 Hz. The relatively low maximum frequency was selected to reduce the possible contributions of local site effects (Bindi et al., 2011) to the source inversion modeling. They interpolated

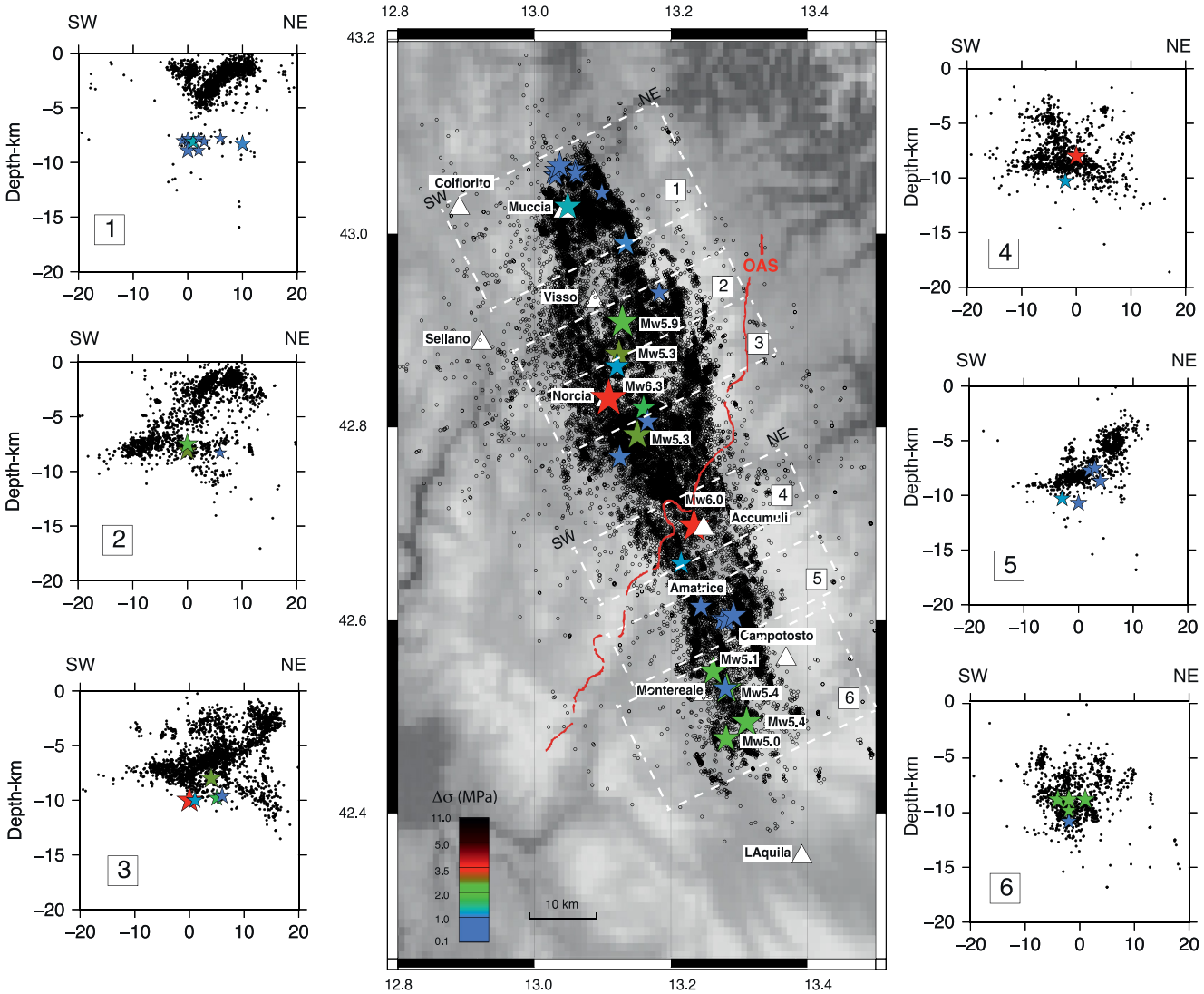

Figure 9. Map view of the relocated aftershocks (black dots) with overlapped the stress drop estimates (colored stars) from the spectral fitting analysis. In the map, the color scale of the stress drop symbols corresponds to the stress drop values. Red lines represent the OAS (Olevano-Antrodoco-Sibillini) thrust front trace (modified after Centamore & Rossi, 2009). White dashed boxes represent the sections reported in the right sides. The cross sections are oriented orthogonally to the strike (155°) direction. For each section the hypocentral locations (colored stars) are shown. The cross sections contain all events within 5 km of distance from the center of each section, except for the southernmost and northernmost cross sections (respectively number 1 and 6), where we project all the events that occurred within 10 km of distance, respectively, to the south and to the north.

their resulting slip distributions to a 0.5 × 0.5 km subfault grid. The resulting moment rate functions (calculated by summing the slip over the fault in each time step), their displacement spectra, and the slip distributions are plotted in Figures 10 and 11. Both of these very similar magnitudes, $M \sim 6$, earthquakes exhibit some source complexity. These two earthquakes therefore provide an excellent opportunity to investigate what a spectral stress drop estimate represents when an earthquake is not a simple circular source. The Amatrice earthquake consists of two distinct, subevents and the total rupture area is larger than that of the Visso earthquake. The slip in the Visso earthquake was more focused into one region, and the maximum slip slightly higher than that in the Amatrice earthquake. These observations are the opposite to those predicted by the spectral stress drop modeling; the Amatrice earthquake has a higher spectral stress drop than the Visso earthquake which would imply a smaller rupture area and a higher average slip because of their similar moment.

Estimating the area, mean slip and stress drop of a heterogeneous slip distribution is not simple as it depends on the area selected and the weighting used (e.g., Noda et al., 2013; Ye et al., 2016). Here we follow the approach

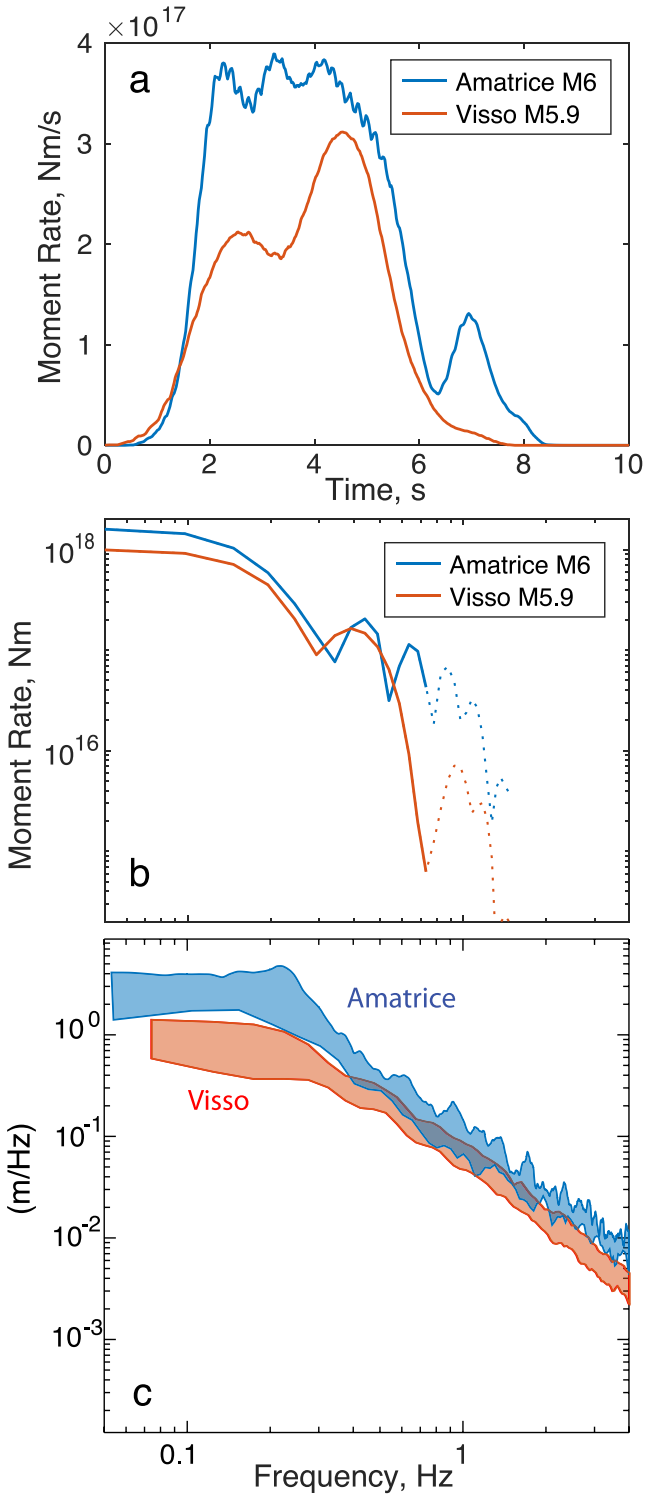

Figure 10. Moment Rate functions (a) and spectra (b) of the Amatrice and Visso earthquakes from data and from slip inversion models of Tinti et al. (2016) and Chiaraluce et al. (2017). Dotted lines indicate extension beyond the band-pass filter used in the slip inversions. (c) Kappa-corrected source spectra for the two earthquakes from this study (± 1 std about mean).

of Brown et al. (2015) to calculate the average values of slip within a range of different slip contours to ensure we have comparable reliable relative estimates. The mean slip for the areas defined by all the selected slip contours is higher for the Visso earthquake than the Amatrice, see Table S5 in Supporting Information S2, and the corresponding areas are larger for the Amatrice earthquake.

The moment rate function of the Amatrice earthquake has a longer duration (confirmed by the dynamic modeling, Gallovič et al., 2019), consistent with the larger rupture area of slip in the finite fault inversion, compared to the Visso earthquake. The effective source dimensions calculated following Mai and Beroza (2000) and Thingbaijam and Mai (2016) are also larger for the Amatrice earthquake than the Visso. Again, these observations are the opposite of the relative values predicted from the spectral stress drop modeling. However, the spectrum of the model of the Amatrice earthquake contains more high-frequency energy than the model of the Visso earthquake, which is consistent with the higher corner frequency calculated for the Amatrice earthquake in almost all spectral studies (Figure 8) and indicates how source complexity can affect spectral modeling. The circular rupture areas predicted by the different spectral models are also shown, with that predicted for the Visso earthquake typically larger than for Amatrice in contrast to the relative size of the finite fault rupture areas.

To investigate further the relationship between the different models, we use the method of Ripperger and Mai (2004) to calculate the stress release on the fault plane in the two earthquakes from the finite fault models. As expected, the Visso earthquake has a larger, more concentrated area of high stress drop (Figure 11), and a higher slip-weighted mean stress drop (following Noda et al., 2013) of 4.8 MPa compared to 2.9 Mpa for the Amatrice earthquake.

This comparison is consistent with the work of Lin and Lapusta (2018), Gallovič and Valentová (2020) and Liu et al. (2023), implying that source complexity can significantly distort spectral measurements of absolute, and relative stress drop that depend on the assumption of simple source models. In this case of two similar-sized earthquakes, the spectral source estimates find the Amatrice to have a smaller rupture area, and higher average slip, whereas the kinematic finite fault inversions reveal the opposite. The consistency of the measurements is more reliable than the absolute numbers. This implies that a higher corner frequency and higher spectral stress drop may indicate slip heterogeneity and other source complexity rather than high localized stress release, In such cases, a higher corner frequency and higher spectral stress drop cannot be simply interpreted in terms of source physics. Finite fault analysis of exceptionally well-recorded smaller earthquakes (e.g., Pennington, Chang, et al., 2022; Pennington, Uchide, & Chen, 2022) also reveal similar slip indicating that even our smaller magnitude measurements may not be well approximated by the circular or point source approximation. The complex spectral shapes we observe in the spectral ratios, and the evidence for azimuthal directivity in the smaller, and even the EGF earthquakes (Figures S4 and S5 in Supporting Information S1) also support the inference that source complexity cannot be ignored for any of the earthquakes considered here. Abercrombie (2021) also showed how a complex source recorded in a limited frequency bandwidth, typical of many spectral studies, can produce an artificial increase in stress drop with seismic moment. This supports the need to keep an open mind concerning the resolution of stress drop scaling in the 2016–2017 Italy earthquake sequence. However, since it is the high frequency radiation which causes the peak ground accelerations, a

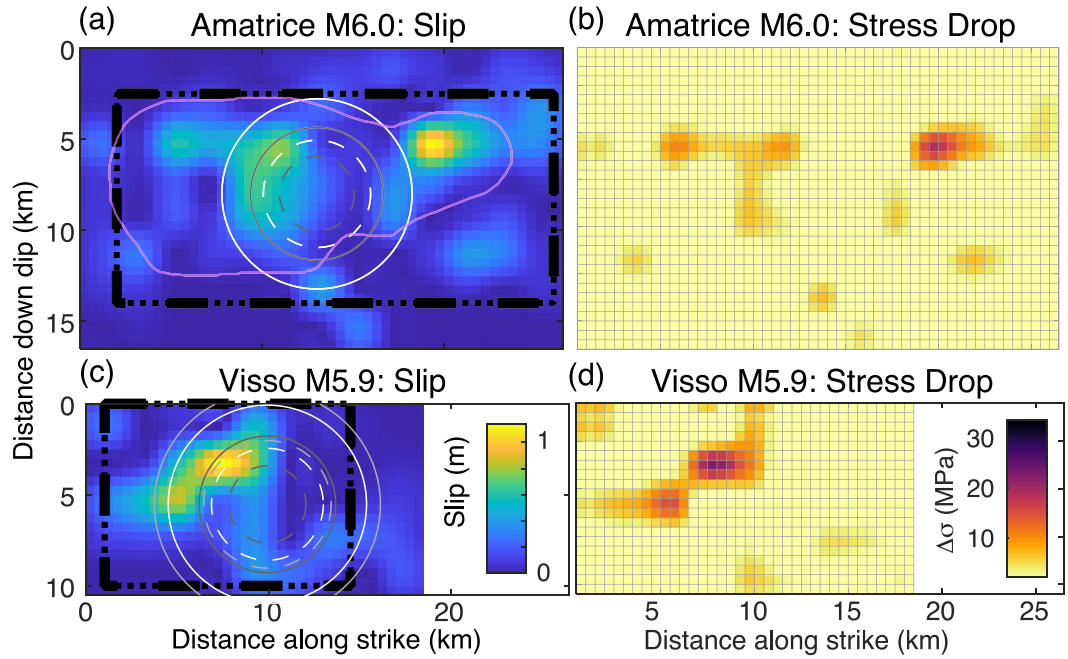

Figure 11. Comparison of spectral results with kinematic finite fault models of Tinti et al. (2016) and Chiaraluce et al. (2017). (a) Slip distribution of the Amatrice earthquake overlain with circles indicating the area of the spectral source dimensions (solid following Brune, 1970; dashed following Madariaga, 1976): spectral fitting (white), spectral ratio (pale gray) and Bindi et al. (dark gray). Black dashed lines are effective source dimensions calculated from the finite fault models following Mai and Beroza (2000) and Thingbaijam and Mai (2016). Pink contour outlines the slip distribution from the dynamic models of Gallovič et al. (2019), for comparison. (b) Stress drop calculated from kinematic finite fault model following Ripperger and Mai (2004). Panel (c, d) as panel (a) and (b) but for the Visso earthquake, to the same scale.

high Brune-style stress drop from spectral modeling may be a more reliable indicator of strong ground motions, whether they be caused by a concentrated area of high slip, or a more distributed complex rupture.

5. Conclusions

We analyze 30 of the larger earthquakes in the central Italy sequence of 2016–2017, to estimate spectral stress drop using two different approaches, and varying the various data selections and assumptions involved. We then compare and interpret our results in comparison with the previously published results, allowing us to separate more reliably real source variability from the large uncertainties.

We find significant uncertainties in stress drop estimates are the product of many different causes, including choice of the magnitude catalog, frequency and width, ambiguities in separating source and path, trade-offs between source, path and site effects, and assumption of a simplified source model. For these reasons, we find wide variation in absolute stress drop estimates, even when assuming the same source model constants.

Relative parameter observations that are consistent across multiple studies are the most reliable. It is encouraging that some events are found to have higher or lower spectral stress drop estimates across multiple studies implying that they represent real variability. Our results support the previously reported spatial variation (Kemna et al., 2021), with decreased stress drop to the south of the OAS thrust front.

Varying levels of correlation between stress drop and magnitude are observed using different methods, magnitude ranges and selections of earthquakes. All results presented here show some increase in stress drop with magnitude; the SR method results in a lower scaling dependence than the spectral fitting. Whether this dependence is real or a consequence of unmodelled source complexity combined with limited frequency range is still unclear.

Through the comparison between the two earthquakes with similar magnitude, Amatrice and Visso seismic events, we deduce that source complexity can significantly distort spectral measurements of absolute, and relative stress drop that assume simple source models. Higher spectral stress drop estimates may represent better strong ground movements and be less directly related to source physics.

There is clearly still much work to do to understand what a spectral stress drop estimate really means, and what the real uncertainties are. Using multiple approaches, and only interpreting consistent results (e.g., Pennington et al., 2021) remains the most reliable way forward at present. The ongoing community stress drop validation study should also provide clarification of these important questions (e.g., Baltay et al., 2022).

Data Availability Statement

The seismic data used here are recorded by the INGV and are accessible from the European Integrated Data Archive (EIDA), INGV Seismological Data Centre (2006, https://doi.org/10.13127/SD/X0FXNH7QFY). The local magnitudes are from the Italian Seismological Instrumental and Parametric Data-Base (http://iside.rm.ingv.it/) through the event selection via interactive map for region shown in Figure 1. The Moment tensors from Herrmann and Malagnini are available from https://www.eas.slu.edu/eqc/eqc_mt/MECH.IT/#DETAILS, and the moment tensors from Scognamiglio are available at http://terremoti.ingv.it/tdmt. The finite fault models from Chiaraluce et al. (2017), were provided by E. Tinti, and we gratefully acknowledge her assistance in analyzing and interpreting these models. The SAC software (Goldstein et al., 2003) was used for routine seismogram processing.

Acknowledgments
This study was supported by the "Real-time Earthquake Risk Reduction for a Resilient Europe" (RISE) project, funded by the European Union's Horizon 2020 research and innovation program (Grant Agreement No. 821115). This material is based upon work supported by the National Science Foundation under Grant EAR 2043281 to Abercrombie.

References

Abercrombie, R. E. (1995). Earthquake source scaling relationships from −1 to 5 using seismograms recorded at 2.5-km depth. *Journal of Geophysical Research*, *120*(6), 4263–4277. https://doi.org/10.1002/2015JB011984

Abercrombie, R. E. (2013). Comparison of direct and coda wave stress drop measurements for the Wells, Nevada, earthquake sequence. *Journal of Geophysical Research: Solid Earth*, *118*(4), 1458–1470. https://doi.org/10.1029/2012JB009638

Abercrombie, R. E. (2014). Stress drops of repeating earthquakes on the San Andreas fault at Parkfield. *Geophysical Research Letters*, *41*(24), 8784–8791. https://doi.org/10.1002/2014GL062079

Abercrombie, R. E. (2015). Investigating uncertainties in empirical Green's function analysis of earthquake source parameters. *Journal of Geophysical Research: Solid Earth*, *100*(B12), 24015–24036. https://doi.org/10.1002/2015jb011984

Abercrombie, R. E. (2021). Resolution and uncertainties in estimates of earthquake stress drop and energy release. *Philosophical Transactions of the Royal Society A*, *379*(2196), 20200131. https://doi.org/10.1098/rsta.2020.0131

Abercrombie, R. E., Chen, X., & Zhang, J. (2020). Repeating earthquakes with remarkably repeatable ruptures on the San Andreas fault at Parkfield. *Geophysical Research Letters*, *47*(23), e2020GL089820. https://doi.org/10.1029/2020GL089820

Abercrombie, R. E., & Rice, J. R. (2005). Can observations of earthquake scaling constrain slip weakening? *Geophysical Journal International*, *162*(2), 406–424. https://doi.org/10.1111/j.1365-246x.2005.02579.x

Abercrombie, R. E., Trugman, D. T., Shearer, P. M., Chen, X., Zhang, J., Pennington, C. N., et al. (2021). Does earthquake stress drop increase with depth? *Journal of Geophysical Research: Solid Earth*, *126*(10), e2021JB022314. https://doi.org/10.1029/2021JB022314

Anderson, J. G., & Hough, S. E. (1984). A model for the shape of the Fourier amplitude spectrum of acceleration at high frequencies. *Bulletin of the Seismological Society of America*, *74*, 1969–1993.

Baltay, A., Abercrombie, R. E., & Taira, T. (2022). The SCEC/USGS community stress drop validation study using the 2019 Ridgecrest earthquake sequence data. *Seismic Research Letters*, *93*, 1252.

Barchi, M. R., Carboni, F., Michele, M., Ercoli, M., Giorgetti, C., Porreca, M., et al. (2021). The influence of subsurface geology on the distribution of earthquakes during the 2016–2017 Central Italy seismic sequence. *Tectonophysics*, *807*, 228797. https://doi.org/10.1016/j.tecto.2021.228797

Bindi, D., Hoby, N. T., RazafindrakotoPicozzi, M., & Oth, A. (2021). Stress drop derived from spectral analysis considering the hypocentral depth in the attenuation model: Application to the Ridgecrest region, California. *Bulletin of the Seismological Society of America*, *111*(6), 3175–3188. https://doi.org/10.1785/0120210039

Bindi, D., Luzi, L., Parolai, S., Di Giacomo, D., & Monachesi, G. (2011). Site effects observed in alluvial basins: The case of Norcia (central Italy). *Bulletin of Earthquake Engineering*, *9*(6), 1941–1959. https://doi.org/10.1007/s10518-011-9273-3

Bindi, D., Spallarossa, D., Picozzi, M., & Morasca, P. (2020). Reliability of source parameters for small events in central Italy: Insights from spectral decomposition analysis applied to both synthetic and real data. *Bulletin of the Seismological Society of America*, *110*(6), 3139–3157. https://doi.org/10.1785/0120200126

Bindi, D., Zaccarelli, R., & Kotha, S. R. (2020). Local and moment magnitude analysis in the Ridgecrest region, California: Impact on Interevent ground-motion variability. *Bulletin of the Seismological Society of America*, *111*(1), 339–355. https://doi.org/10.1785/0120200227

Boore, D. M., & Boatwright, J. (1984). Average body-wave radiation coefficients. *Bulletin of the Seismological Society of America*, *74*(5), 1615–1621. https://doi.org/10.1785/bssa0740051615

Brown, L., Wang, K., & Sun, T. (2015). Static stress drop in the M_w 9 Tohoku-oki earthquake: Heterogeneous distribution and low average value. *Geophysical Research Letters*, *42*(24), 10595–10600. https://doi.org/10.1002/2015GL066361

Brune, J. N. (1970). Tectonic stress and the spectra of seismic shear waves from earthquakes. *Journal of Geophysical Research*, *75*(26), 4997–5009. https://doi.org/10.1029/jb075i026p04997

Brune, J. N. (1971). Correction (to Brune 1970). *Journal of Geophysical Research*, *76*, 5002.

Calderoni, G., Rovelli, A., Ben-Zion, Y., & Di Giovambattista, R. (2015). Along-strike rupture directivity of earthquakes of the 2009 L'Aquila, central Italy, seismic sequence. *Geophysical Journal International*, *203*(1), 399–415. https://doi.org/10.1093/gji/ggv275

Calderoni, G., Rovelli, A., & Di Giovambattista, R. (2010). Large amplitude variations recorded by an on-fault seismological station during the L'Aquila earthquakes: Evidence for a complex fault-induced site effect. *Geophysical Research Letters*, *37*(24), L24305. https://doi.org/10.1029/2010GL045697

Calderoni, G., Rovelli, A., & Di Giovambattista, R. (2017). Rupture directivity of the strongest 2016–2017 central Italy earthquakes. *Journal of Geophysical Research: Solid Earth*, *122*(11), 9118–9131. https://doi.org/10.1002/2017JB014118

Calderoni, G., Rovelli, A., & Di Giovambattista, R. (2019). Stress drop, apparent stress, and radiation efficiency of clustered earthquakes in the nucleation volume of the 6 April 2009, M_w 6.1 L'Aquila earthquake. *Journal of Geophysical Research: Solid Earth*, *124*(10), 10360–10375. https://doi.org/10.1029/2019JB017513

Calderoni, G., Rovelli, A., & Singh, S. K. (2013). Stress drop and source scaling of the 2009 April L'Aquila earthquakes. *Geophysical Journal International*, *192*(1), 260–264. https://doi.org/10.1093/gji/ggs011

Centamore, E., & Rossi, D. (2009). Neogene-quaternary tectonics and sedimentation in the central Apennines. *Bollettino della Societa Geologica Italiana*, *128*(1), 73–88.

Chen, X., & Abercrombie, R. E. (2020). Improved approach for stress drop estimation and its application to an induced earthquake sequence in Oklahoma. *Geophysical Journal International*, *223*(1), 233–253. https://doi.org/10.1093/gji/ggaa316

Chiaraluce, L., Di Stefano, R., Tinti, E., Scognamiglio, L., Michele, M., Casarotti, E., et al. (2017). The 2016 central Italy seismic sequence: A first look at the mainshocks, aftershocks, and source models. *Seismological Research Letters*, *88*(3), 757–771. https://doi.org/10.1785/0220160221

Cocco, M., Tinti, E., & Cirella, A. (2016). On the scale dependence of earthquake stress drop. *Journal of Seismology*, *20*(4), 1151–1170. https://doi.org/10.1007/s10950-016-9594-4

Colavitti, L., Lanzano, G., Sgobba, S., Pacor, F., & Gallovič, F. (2022). Empirical evidence of frequency dependent directivity effects from mall-to-moderate normal fault earthquakes in Central Italy. *Journal of Geophysical Research: Solid Earth*, *127*(6), e2021JB023498. https://doi.org/10.1029/2021JB023498

Dreger, D. S., Gee, L., Lombard, P., Murray, M. H., & Romanowicz, B. (2005). Rapid finite-source analysis and near-fault strong ground motions: Application to the 2003 M_w 6.5 San Simeon and 2004 M_w 6.0 Parkfield earthquakes. *Seismological Research Letters*, *76*(1), 40–48. https://doi.org/10.1785/gssrl.76.1.40

Dreger, D. S., & Kaverina, A. (2000). Seismic remote sensing for the earthquake source process and near-source strong shaking: A case study of the October 16, 1999 Hector mine earthquake. *Geophysical Research Letters*, *27*(13), 1941–1944. https://doi.org/10.1029/1999GL011245

Eshelby, J. (1957). The elastic field of an ellipsoid inclusion and related problems. *Proceedings of The Royal Society*, *241*(1226), 376–396.

Gallovič, F., & Valentová, Ľ. (2020). Earthquake stress drops from dynamic rupture simulations constrained by observed ground motions. *Geophysical Research Letters*, *47*(4), e2019GL085880. https://doi.org/10.1029/2019GL085880

Gallovič, F., Valentová, Ľ., Ampuero, J.-P., & Gabriel, A.-A. (2019). Bayesian dynamic finite-fault inversion: 2. Application to the 2016 M_w 6.2 Amatrice, Italy, earthquake. *Journal of Geophysical Research: Solid Earth*, *124*(7), 6970–6988. https://doi.org/10.1029/2019JB017512

Goldstein, P., Dodge, D., Firpo, M., & Minner, L. (2003). SAC2000: Signal processing and analysis tools for seismologists and engineers. In W. H. K. Lee, H. Kanamori, P. C. Jennings, & C. Kisslinger (Eds.), *Invited contribution to 'the IASPEI international handbook of earthquake and engineering seismology'*. Academic Press.

Hartzell, S. H., & Heaton, T. H. (1983). Inversion of strong ground motion and teleseismic waveform data for the fault rupture history of the 1979 Imperial Valley, California, earthquake. *Bulletin of the Seismological Society of America*, *73*(6A), 1553–1583. https://doi.org/10.1785/bssa07306a1553

Herrmann, R., Malagnini, L., & Munafò, I. (2011). Regional moment tensors of the 2009 L'Aquila earthquake sequence. *Bulletin of the Seismological Society of America*, *101*(3), 975–993. https://doi.org/10.1785/0120100184

Ide, S., & Beroza, G. C. (2001). Does apparent stress vary with earthquake size? *Geophysical Research Letters*, *28*(17), 3349–3352. https://doi.org/10.1029/2001gl013106

Ide, S., Beroza, G. C., Prejean, S. G., & Ellsworth, W. L. (2003). Apparent break in earthquake scaling due to path and site effects on deep borehole recordings. *Journal of Geophysical Research*, *108*, 2271. https://doi.org/10.1029/2001JB001617

INGV Seismological Data Centre. (2006). *Rete Sismica Nazionale (RSN)*. Istituto Nazionale di Geofisica e Vulcanologia (INGV). https://doi.org/10.13127/SD/X0FXNH7QFY

Ji, C., & Archuleta, R. J. (2020). Two empirical double-corner-frequency source spectra and their physical implications. *Bulletin of the Seismological Society of America*, *111*(2), 737–761. https://doi.org/10.1785/0120200238

Ji, C., & Archuleta, R. J. (2022). A source physics interpretation of nonself-similar double-corner-frequency source spectral model JA19_2S. *Seismological Research Letters*, *93* (2A), 777–786. https://doi.org/10.1785/0220210098

Kanamori, H., & Brodsky, E. (2004). The physics of earthquakes. *Reports on Progress in Physics*, *67*(8), 1429–1496. https://doi.org/10.1088/0034-4885/67/8/r03

Kaneko, Y., & Shearer, P. M. (2014). Seismic source spectra and estimated stress drop from cohesive-zone models of circular subshear rupture. *Geophysical Journal International*, *197*(2), 1002–1015. https://doi.org/10.1093/gji/ggu030

Kaneko, Y., & Shearer, P. M. (2015). Variability of seismic source spectra, estimated stress drop, and radiated energy, derived from cohesive zone models of symmetrical and asymmetrical circular and elliptical ruptures. *Journal of Geophysical Research: Solid Earth*, *120*(2), 1053–1079. https://doi.org/10.1002/2014JB011642

Keilis-Borok, V. (1959). On estimation of the displacement in an earthquake source and of source dimensions. *Annali di. Geofisisica*, *12*, 205–214. https://doi.org/10.4401/ag-5718

Kemna, K. B., Verdecchia, A., & Harrington, R. M. (2021). Spatio-temporal evolution of earthquake static stress drop values in the 2016–2017 central Italy seismic sequence. *Journal of Geophysical Research: Solid Earth*, *126*(11), e2021JB022566. https://doi.org/10.1029/2021JB022566

Lin, Y.-Y., & Lapusta, N. (2018). Microseismicity simulated on asperity-like fault patches: On scaling of seismic moment with duration and seismological estimates of stress drops. *Geophysical Research Letters*, *45*(16), 8145–8155. https://doi.org/10.1029/2018GL078650

Liu, M., Huang, Y., & Ritsema, J. (2023). Characterizing multisubevent earthquakes using the Brune source model. *Bulletin of the Seismological Society of America*, *113*(2), 577–591. https://doi.org/10.1785/0120220192

Madariaga, R. (1976). Dynamics of an expanding circular crack. *Bulletin of the Seismological Society of America*, *66*(3), 639–666. https://doi.org/10.1785/bssa0660030639

Madariaga, R. (1979). On the relation between seismic moment and stress drop in the presence of stress and strength heterogeneity. *Journal of Geophysical Research*, *84*(B5), 2243–2250. https://doi.org/10.1029/JB084IB05P02243

Mai, P. M., & Beroza, G. C. (2000). Source scaling properties from finite-fault-rupture models. *Bulletin of the Seismological Society of America*, *90*(3), 604–615. https://doi.org/10.1785/0119990126

Mai, P. M., & Thingbaijam, K. K. S. (2014). SRCMOD: An online database of finite-fault rupture models. *Seismological Research Letters*, *85*(6), 1348–1357. https://doi.org/10.1785/0220140077

Mayeda, K., Hofstetter, A., O'Boyle, J. L., & Walter, W. R. (2003). Stable and transportable regional magnitudes based on coda-derived moment rate spectra. *Bulletin of the Seismological Society of America*, *93*(1), 224–239. https://doi.org/10.1785/0120020020

Mayeda, K., Malagnini, L., & Walter, W. R. (2007). A new spectral ratio method using narrow band coda envelopes: Evidence for non-self similarity in the Hector mine sequence. *Geophysical Research Letters*, *34*(11), L11303. https://doi.org/10.1029/2007GL030041

Michele, M., Chiaraluce, L., Di Stefano, R., & Waldhauser, F. (2020). Fine-scale structure of the 2016–2017 Central Italy seismic sequence from data recorded at the Italian National Network. *Journal of Geophysical Research: Solid Earth*, *125*(4), e2019JB018440. https://doi.org/10.1029/2019JB018440

Morasca, P., Bindi, D., Mayeda, K., Roman-Nieves, J., Barno, J., Walter, W. R., & Spallarossa, D. (2022). Source scaling comparison and validation in central Italy: Data intensive direct *S* waves versus the sparse data coda envelope methodology. *Geophysical Journal International*, *231*(3), 1573–1590. https://doi.org/10.1093/gji/ggac268

Morasca, P., Walter, W. R., Mayeda, K., & Massa, M. (2019). Evaluation of earthquake stress parameters and its scaling during the 2016–2017 Amatrice-Norcia-Visso sequence—Part I. *Geophysical Journal International*, *218*(1), 446–455. https://doi.org/10.1093/gji/ggz165

Moyer, P. A., Boettcher, M. S., McGuire, J. J., & Collins, J. A. (2018). Spatial and temporal variations in earthquake stress drop on Gofar Transform Fault, East Pacific Rise: Implications for fault strength. *Journal of Geophysical Research: Solid Earth*, *123*(9), 7722–7740. https://doi.org/10.1029/2018JB015942

Noda, H., Lapusta, N., & Kanamori, H. (2013). Comparison of average stress drop measures for ruptures with heterogeneous stress change and implications for earthquake physics. *Geophysical Journal International*, *193*(3), 1691–1712. https://doi.org/10.1093/gji/ggt074

Pennington, C. N., Chang, H., Rubinstein, J. L., Abercrombie, R. E., Nakata, N., Uchide, T., & Cochran, E. S. (2022). Quantifying the sensitivity of microearthquake slip inversions to station distribution using a dense nodal Array. *Bulletin of the Seismological Society of America*, *112* (3), 1252–1270. https://doi.org/10.1785/0120210279

Pennington, C. N., Chen, X., Abercrombie, R. E., & Wu, Q. (2021). Cross validation of stress drop estimates and interpretations for the 2011 Prague, OK, earthquake sequence using multiple methods. *Journal of Geophysical Research: Solid Earth*, *126*(3), e2020JB020888. https://doi.org/10.1029/2020JB020888

Pennington, C. N., Uchide, T., & Chen, X. (2022). Slip characteristics of induced earthquakes: Insights from the 2015 M_w 4.0 Guthrie, Oklahoma earthquake. *Journal of Geophysical Research: Solid Earth*, *127*(5), e2021JB023564. https://doi.org/10.1029/2021JB023564

Ripperger, J., & Mai, P. M. (2004). Fast computation of static stress changes on 2D faults from final slip distributions. *Geophysical Research Letters*, *31*(18), L18610. https://doi.org/10.1029/2004GL020594

Rovelli, A., & Calderoni, G. (2014). Stress drops of the 1997–1998 Colfiorito, central Italy earthquakes: Hints for a common behaviour of normal-faults in the Apennines. *Pure and Applied Geophysics*, *171*(10), 2731–2746. https://doi.org/10.1007/s00024-014-0856-1

Ruhl, C. J., Abercrombie, R. E., & Smith, K. D. (2017). Spatiotemporal variation of stress drop during the 2008 Mogul, Nevada, earthquake swarm. *Journal of Geophysical Research: Solid Earth*, *122*(10), 8163–8818. https://doi.org/10.1002/2017jb014601

Scognamiglio, L., Tinti, E., Casarotti, E., Pucci, S., Villani, F., Cocco, M., et al. (2018). Complex fault geometry and rupture dynamics of the M_W 6.5, 30 October 2016, central Italy earthquake. *Journal of Geophysical Research: Solid Earth*, *123*(4), 2943–2964. https://doi.org/10.1002/2018JB015603

Scognamiglio, L., Tinti, E., Michelini, A., Dreger, D., Cirella, A., Cocco, M., et al. (2010). Fast determination of moment tensors and rupture history: What has been learned from the 6 April 2009 L'Aquila earthquake sequence. *Seismological Research Letters*, *81*, 892–906. https://doi.org/10.1785/gssrl.81.6.892

Selvadurai, P. A. (2019). Laboratory insight into seismic estimates of energy partitioning during dynamic rupture: An observable scaling breakdown. *Journal of Geophysical Research: Solid Earth*, *124*(11), 11350–11379. https://doi.org/10.1029/2018JB017194

Shearer, P. M., Abercrombie, R. E., Trugman, D. T., & Wang, W. (2019). Comparing EGF methods for estimating corner frequency and stress drop from *P*-wave spectra. *Journal of Geophysical Research: Solid Earth*, *124*(4), 3966–3986. https://doi.org/10.1029/2018JB016957

Shearer, P. M., Prieto, G. A., & Hauksson, E. (2006). Comprehensive analysis of earthquake source spectra in southern California. *Journal of Geophysical Research*, *111*(B6), 693. https://doi.org/10.1029/2005jb003979

Singh, S. K., Apsel, R., Fried, J., & Brune, J. N. (1982). Spectral attenuation of SH-waves along Imperial fault. *Bulletin of the Seismological Society of America*, *101*(6A), 2003–2016. https://doi.org/10.1785/bssa07206a2003

Thingbaijam, K. K. S., & Mai, P. M. (2016). Evidence for truncated exponential probability distribution of earthquake slip. *Bulletin of the Seismological Society of America*, *106*(4), 1802–1816. https://doi.org/10.1785/0120150291

Tinti, E., Casarotti, E., Ulrich, T., Taufiqurrahman, T., Li, D., & Gabriel, A. (2021). Constraining families of dynamic models using geological, geodetic and strong ground motion data: The M_w 6.5, October 30th, 2016, Norcia earthquake, Italy. *Earth and Planetary Science Letters*, *576*, 117237. https://doi.org/10.1016/j.epsl.2021.117237

Tinti, E., Scognamiglio, L., Michelini, A., & Cocco, M. (2016). Slip heterogeneity and directivity of the M_L 6.0, 2016, Amatrice earthquake estimated with rapid finite-fault inversion. *Geophysical Research Letters*, *43*(20), 10745–10752. https://doi.org/10.1002/2016GL071263

Uchide, T., & Imanishi, K. (2016). Small earthquakes deviate from the Omega-square model as revealed by multiple spectral ratio analysis. *Bulletin of the Seismological Society of America*, *106*(3), 1357–1363. https://doi.org/10.1785/0120150322

Walter, W. R., Yoo, S.-H., Mayeda, K., & Gök, R. (2017). Earthquake stress via event ratio levels: Application to the 2011 and 2016 Oklahoma seismic sequences. *Geophysical Research Letters*, *44*(7), 3147–3155. https://doi.org/10.1002/2016GL072348

Wang, H., Ren, Y., Wen, R., & Xu, P. (2019). Breakdown of earthquake self-similar scaling and source rupture directivity in the 2016–2017 central Italy seismic sequence. *Journal of Geophysical Research: Solid Earth*, *124*(4), 3898–3917. https://doi.org/10.1029/2018JB016543

Yamada, T., Mori, J. J., Ide, S., Kawakata, H., Iio, Y., & Ogasawara, H. (2005). Radiation efficiency and apparent stress of small earthquakes in a South African gold mine. *Journal of Geophysical Research*, *110*(B1), B01305. https://doi.org/10.1029/2004JB003221

Ye, L., Lay, T., Kanamori, H., & Rivera, L. (2016). Rupture characteristics of major and great ($M_w \geq 7.0$) megathrust earthquakes from 1990 to 2015: 1. Source parameter scaling relationships. *Journal of Geophysical Research: Solid Earth*, *121*(2), 826–844. https://doi.org/10.1002/2015jb012426

Yoshimitsu, N., Ellsworth, W. L., & Beroza, G. C. (2019). Robust stress drop estimates of potentially induced earthquakes in Oklahoma: Evaluation of empirical Green's function. *Journal of Geophysical Research: Solid Earth*, *124*(6), 5854–5866. https://doi.org/10.1029/2019JB017483